ABSTRACT

RENDE, CRAIG MICHAEL. Experimental Investigation on a 392 Series, High Performance Heat Sink. (Under the direction of Professor Richard D. Gould.)

The primary focus of this research was to experimentally obtain the performance of a Wakefield 392 series heat sink by conducting free and forced convection tests. By measuring the steady-state maximum temperature for various geometric orientations, Nusselt number correlations were found experimentally. These correlations can now be used to predict the performance of the heat sink. It was found that the experimental Nusselt number correlations can predict the performance of the heat sink within 10%. Furthermore, steady-state maximum temperature results showed that for slow fan speeds (2m/s-3m/s), the heat sink temperature achieved a value no higher than 80°C, while dissipating 150 watts. Furthermore, it was found that for a dual heat sink, forced convection test, where one heat sink was downstream from the other, any gap spacing between the devices had minimal effect on the overall thermal performance. Finally, ANSYS® and SolidWorks® were used to geometrically optimize a four-chip power source on a copper heat spreader. Results showed the spreader should carry a thickness of 5-10mm, while the surface area of the power chips should be as large as possible. Furthermore, the spacing between the chips was found to be unimportant. By finding thermal optimization of a heat spreader, and combining it to a system with a heat sink that has also been thermally optimized, a complete system can be designed with optimal performance.

Heat Transfer Analysis on Various Thermal Dissipation Devices

by
Craig Michael Rende

A thesis submitted to the Graduate Faculty of
North Carolina State University
in partial fulfillment of the
requirements for the degree of
Master of Science

Mechanical Engineering

Raleigh, North Carolina

2009

APPROVED BY:

_____	_____
Dr. Thomas Ward	Dr. Subhashish Bhattacharya

_____
Dr. Richard D. Gould

Chair of Advisory Committee

DEDICATION

I want to dedicate this thesis to my mother, step-father, father, and my best friends who have continually encouraged me throughout my entire educational experience. Without your support and love throughout my entire life, none of this would have ever been possible.

BIOGRAPHY

Craig M. Rende was born in Daytona Beach, Florida on October 9th, 1986. He grew up in Valhalla, NY where he attended Valhalla Middle/High School and graduated in June of 2004. Sports, and especially soccer, became an integral part of his life throughout his teenage years. As his passion for math and science grew, he attended Manhattan College and studied Mechanical Engineering. In May of 2008, he graduated with a Bachelor's in Science of Mechanical Engineering at the top of his class. At the completion of his Bachelors Degree, Craig received a full academic scholarship to North Carolina State University. In January of 2009, he began research focused on thermal heat transfer analysis. With the completion of his thesis in December of 2009, Craig received a Masters Degree in Mechanical Engineering.

ACKNOWLEDGMENTS

I would like to thank my advisor Dr. Richard Gould for the opportunity and continual help throughout the entire time we worked together. I would also like to thank Dr. Subhashish Bhattacharya and Dr. Thomas Ward for being on my committee. Much thanks and gratitude goes out to the entire Mechanical Engineering Department, especially Mrs. Crystal Hanson and Miss. Toni Rand for having a daily positive influence on my research. Finally, I would like to thank my friends and family for being there for me throughout my entire stay down at North Carolina State University.

TABLE OF CONTENTS

LIST OF FIGURES

LIST OF TABLES

Chapter 1

Introduction

1.1 Background

A heat sink is a device that is used to cool many various types of electronic devices by absorbing and dissipating the heat the device produces through direct contact. Heat sinks are an extremely useful component that can be used to drastically lower the maximum temperature of electronic devices, as well as increase their overall thermal efficiency and performance.

A heat sink works on the basis of transferring heat from a high temperature source to a lower temperature source, where the lower temperature source has a much greater heat capacity. Furthermore, it is desired to have a transfer in thermal energy from the high temperature electronic device into the heat sink (low temperature source). The hope is to produce a system which reaches thermal equilibrium rapidly, by using the most efficient heat sink possible [1].

Most heat sinks are metal devices which contain a base in the shape of a flat surface. On top of this flat base, a large number of thin, fin like protrusions extend out of the flat surface of the device. These fins produce a high surface area, which reduces the thermal resistance and enhances the cooling for the primary electronic device. Heat sinks used in combination with a fan will produce a more thermally efficient system. The goal is to attain

the lowest maximum device temperature possible. Throughout this study, both free and forced convection heat sink performance will be considered, with the focus centered on the latter.

1.2 Experimental Layout

The organization of this study can be broken into several main components. Firstly, some background regarding geometric heat sink optimization will be discussed. It is pertinent to discuss how heat sink manufacturers optimize their product before fabrication. Since the Wakefield 392-series heat sink is the focal point of this study, it is important to briefly discuss all the geometric parameters that go into optimizing such a product.

Secondly, the experimental work will center on a free-convection test for one heat sink, as well has as forced convection tests. For the forced convection tests, a constant power heat source of 150 watts was geometrically centered on the top of the heat sink, and steady-state temperatures were recorded for various air flow speeds. From this study, maximum temperatures for a forced-convection system were determined. Furthermore, experimentally determined heat transfer parameters were used to derive Nusselt number correlations. From these correlations, the heat sink performance can be predicted for a wide range of operating conditions.

Finally, four constant power sources were symmetrically placed on top of a copper heat spreader (a flat plate). Thermal simulations were run using ANSYS® and SolidWorks® to obtain the optimal geometric orientation for a variety of parameters including heat

spreader thickness, surface area of the power sources, spacing between the power sources, etc… By optimizing a copper heat spreader with multiple power sources, such a device can be placed directly on top of a heat sink to further increase its thermal efficiency. As a result, a large number of heat transfer and geometric parameters have been studied, which will help develop an overall optimal heat sink design.

CHAPTER 2

Previous Study on Heat Sink Optimization

2.1 Point of Emphasis

It is important to note that the study of fin optimization for heat sinks has been done by numerous engineers in the past. Thus, this section will focus on summarizing the pervious mathematical and experimental studies. A basic mathematical derivation to obtain equations for fin performance and fin efficiency will follow. This gives the ability to determine which geometric and material parameters will directly affect the fin design. Furthermore, a previous study where ideal fin geometry was found, will also be discussed.

2.2 Mathematical Analysis

2.2.1 Introduction to Fins

The discussion for fin optimization will begin with a mathematical derivation to obtain the equations for fin effectiveness and efficiency. When the final result is found, this will show the basic parameters which will ultimately help choose an optimal fin design. To begin, a basic fin design having a rectangular profile and cross-section has been chosen, as shown in Figure 2.1:

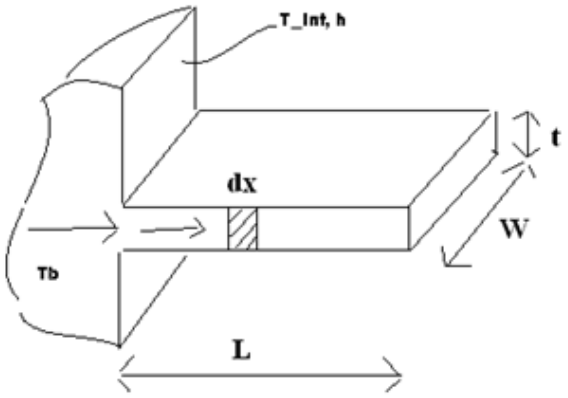

Figure 2.1: Basic fin geometry (where t<<W)

The mathematical derivation to follow will be for a single fin. Therefore, this portion of the analysis will focus on basic parameters such as fin area and perimeter, whereas, the latter experimental study will pertain to things such as the number of fins, fin spacing, fin length, etc…

By focusing on an infinitesimally small portion of the fin, the fin can be analyzed by performing an energy balance on a piece of length dx, shown by [2]:

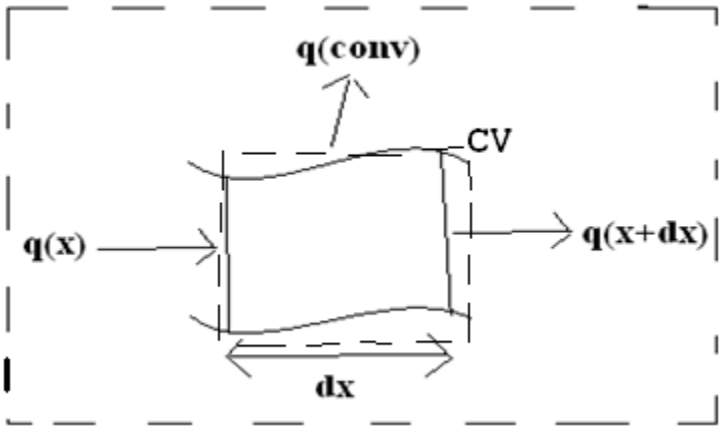

Figure 2.2: Infinitesimally Small Portion of Fin

At any point along the fin, convection and axial conduction are present. Heat is conducted through the fin, while convection is present along the surfaces of the fin. For simplification of the system, some general assumptions can be made:

- ✓ Steady state heat transfer
- ✓ No internal heat generation
- ✓ One-dimensional heat conduction (x-direction)
- ✓ Constant thermal conductivity (k)
- ✓ Constant convection coefficient (h)

2.2.2 Derivation

After making these assumptions, an energy balance can be performed on the control volume. The first step is to define the control volume, which can be seen in Figure 2.2 above. Furthermore, all energy terms present are represented by means of arrows. For heat transfer, energy can be transferred through three modes: conduction, convection, and radiation, and can be added to the system by an external source. For the system at hand, the steady state energy balance gives [2].

$$\dot{E}_{in} = \dot{E}_{out} \tag{2.1}$$

$$q_x = q_{x+dx} + q_{convection} \tag{2.2}$$

Where each of the three energy components can be represented by basic heat transfer equations:

$$q_x = -kA_C\left[\frac{dT}{dx}\right]_X \tag{2.3}$$

$$q_{x+dx} = -kA_c\left[\frac{dT}{dx}\right]_{x+dx} = q_x + \frac{d}{dx}(q_x)dx \tag{2.4}$$

$$q_{conv} = hA_s(T - T_\infty) \tag{2.5}$$

and $A_s = pdx$ (p = perimeter of the fin)

By substituting the above energy components into (2.2), the result yields:

$$kA_C\left[\frac{dT}{dx}\right]_{X+dX} - kA_C\left[\frac{dT}{dx}\right]_X - hpdx(T - T_\infty) = 0 \tag{2.6}$$

Performing a Taylor Series expansion on the first term, then dividing all terms by dx, and noticing that kA_C is a constant gives:

$$\frac{d^2T}{dx^2} - \frac{hp}{kA_c}(T - T_\infty) = 0 \tag{2.7}$$

To further simplify (2.7) another parameter θ can be introduced:

$$\theta = T(x) - T_\infty \tag{2.8}$$

Therefore:

$$\frac{d^2\theta}{dx^2} - m^2\theta = 0 \text{, where } m^2 = \frac{hp}{kA_C} \tag{2.9}$$

Thus, the fin equation in terms of temperature difference can be written as:

$$\frac{d^2\theta}{dx^2} - m^2\theta = 0 \tag{2.10}$$

The solution to this 2nd order homogeneous ordinary differential equation is [2]:

$$\theta(x) = C_1 e^{-mx} + C_2 e^{mx} \tag{2.11}$$

Now that we have a general solution for theta, boundary conditions can be implemented for the derivation. Not restricted to a thin fin, constants C_1 and C_2 can be solved for. At x=0

$$\theta(b) = \theta(0) = C_1 e^{-(m)(0)} + C_2 e^{m(0)} \tag{2.12}$$

Therefore,

$$\theta(b) = C_1 + C_2 \tag{2.13}$$

- For a very long fin, $\theta(L) = 0$, as L→∞. Thus, C_2=0, and C_1=θ_b.

Finally, a distinct equation of theta as a function of x for a long fin can be written as:

$$\theta(x) = \theta_b e^{-mx} \tag{2.14}$$

Equation (2.14) can also be rewritten as:

$$T(x) - T_\infty = (T_b - T_\infty)e^{-mx} \tag{2.15}$$

$$e^{-mx} = \frac{T(x) - T_\infty}{T_b - T_\infty} \; and \; m = \sqrt{\frac{hp}{kA_c}} \tag{2.16}$$

A fundamental equation of heat transfer for heat conduction was shown earlier by $q_x = -kA_C\left[\frac{dT}{dx}\right]$. By taking the derivative of (2.15), we get:

$$q_x = -kA_c(T_b - T_\infty)e^{-mx}(-m) \tag{2.17}$$

plugging in the value for "m" yields:

$$q_x = \sqrt{hpkA_c}(T_b - T_\infty)e^{-mx} \tag{2.18}$$

The conduction into the fin at x = 0, gives the fin heat dissipation.

$$q_{fin} = \sqrt{hpkA_c}(T_b - T_\infty) = \sqrt{hpkA_c}\theta_b \tag{2.19}$$

If the fin is not present, the total heat dissipated can easily be written as [2]:

$$q_{without\ fin} = hA_c(T_b - T_\infty) = hA_c\theta_b \tag{2.20}$$

This derivation was carried out to show that the heat dissipated from a fin is a direct function of k(thermal conductivity) and h (convection coefficient), and simple geometric parameters of p(perimeter) and A_c(area), as shown by (2.19).

As mentioned earlier, fin designers are interested in relations for fin performance and fin efficiency. Fin effectiveness is defined as [2]:

$$\varepsilon = \frac{q_f}{q_{without}} \tag{2.21}$$

Substituting (2.19) and (2.20) into (2.21), fin performance of a long fin can be written as:

$$\varepsilon = \frac{\sqrt{hpkA_C}\theta_b}{hA_C\theta_b} = \sqrt{\frac{pk}{hA_C}} \tag{2.22}$$

This result shows that a few simple parameters described below determine fin performance:

- As the thermal conductivity, k is increased, the fin effectiveness ε increases.
- As the convection coefficient decreases, fin effectiveness ε increases.
- As the ratio of P/A_c is increased, fin effectiveness ε increases. This final statement relates the geometric design of the fin to performance. It is ideal for the perimeter to increase as the fin cross-sectional area is decreased.

Each conclusion drawn will be further examined during the experimental part of this work. Finally, fin efficiency is defined as:

$$\eta_{fin} = \frac{q_f}{q_{\max}} = \frac{\sqrt{hpkA_c}\theta_b}{hpL\theta_b} = \frac{1}{L}\sqrt{\frac{kA_c}{hp}} \tag{2.23}$$

Therefore, it can be shown that fin efficiency is dependent upon the same parameters as fin effectiveness. Evaluating (2.19), (2.20) and (2.22) can be used as a guide to find an optimal fin design.

2.3 Discussion of Previous Heat Sink Study

2.3.1 Background Information:

This section will focus on a discussion of a study by Bibol's and Fijol's [3] for a parallel plate heat sink constrained to various parameters. Some of these factors include the number of fins, fin height, total thermal resistance, base thickness, and fin thickness. The goal is to summarize the controlling parameters that must be considered when choosing an optimal fin design. Furthermore, the expectation is to extend these optimal fin results to a copper base plate heat spreader and chip design in order to design an optimal cooling scheme.

A thorough heat sink analysis involves looking at areas such as fluid, mechanical, and thermal studies. Yet, because the focus is on creating an effectively cooled electronic device, thermal analysis is the main area of focus throughout this section. The goal is to determine optimal numerical values for the important parameters governing the overall cooling performance. Important parameters include fin height and thickness. A range of numerical values for each parameter needs to be validated for practicality of design.

The physical layout of the system needs to be mentioned before the results are discussed. The system under consideration here has a 20mm by 20mm chip that produces 75

watts of power. Also, the heat sink is enclosed at the top and the bottom. A convoluted fin has been attached to the extruded base. These types of fins create the ability to be manufactured at a much smaller thickness (up to 1mm in thickness).

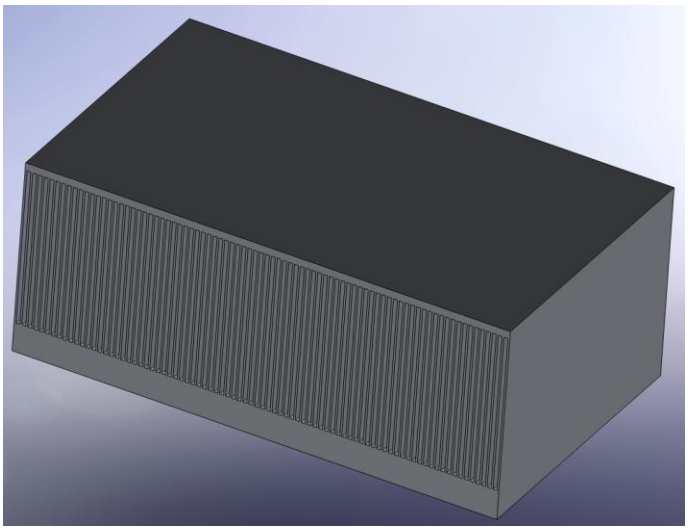

Figure 2.3: Sketch of Convoluted Fin

Whereas, typical extruded heat sink values can range from 1mm-2mm in thickness. In this work, non-dimensional parameters such as thermal resistance to fin thickness, or fin height to fin thickness will be much more practical to obtain numerical results pertaining to our area of study.

2.3.2 Manufacturability

Although focus will not be on manufacturability, it is still essential to mention the typical range of values for actual heat sinks. The table below shows a general range that manufacturers adhere to for fin height, fin thickness, and base thickness [3]:

Table 2.1: Manufacturer Fin Parameters

Fin Height	3-50mm
Base Thickness	3-16mm
Fin thickness (convoluted fin)	.15-.8mm

Still to come in this section is the analysis to select optimal values of fin height, fin thickness, and base thickness. Furthermore, manufacturers do have constraints regarding fin pitch, and the consequent gap spacing vs. fin thickness relation. Figure 2.4 shows the inverse relation between fin thickness and pitch. Companies must stay within certain limitations in that the fin spacing must be larger than a multiple of the fin thickness.

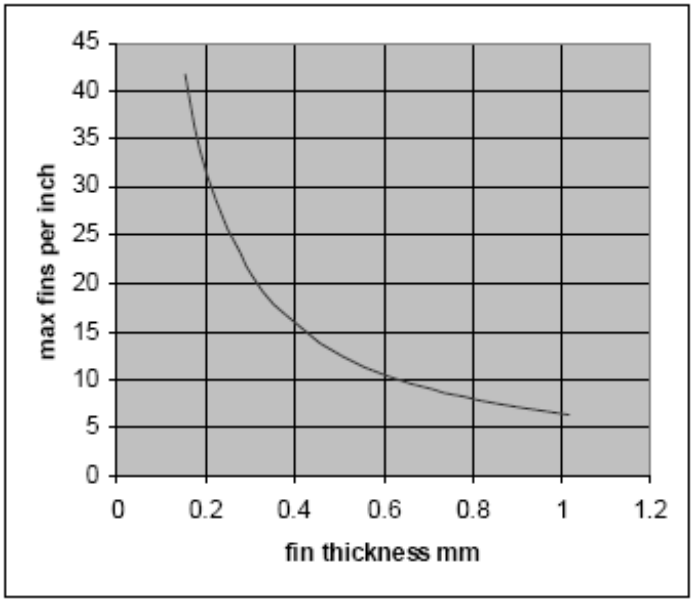

Figure 2.4: Manufactured Fin Density vs. Fin Thickness

For example, fins that have a height from 25-50mm and a width up to 75mm are constrained to a minimum gap of three times the fin thickness because of the extreme constriction of air flow through the heat sink. An example is shown in the table below from Bibir and Fijols' paper [3]:

Table 2.2: Maximum Manufacturability for Fin Density, Gap Spacing, Fin Thickness, and Maximum Fins/Inch

Fin Thickness	**Minimum gap (3x)**	**Max # of Fins for 75 mm H.S. width**	**Max fins/inch**
.3mm	.9mm	62	20.8
.4mm	1.2mm	46	15.6
.5mm	1.5mm	38	12.5
.8mm	2.4mm	24	7.8

In this study, the goal for the thermal resistance value of the system was .27 K/W. Total thermal resistance is due to the sum of the resistances from the air, fin geometric performance, and thermal heat spreading.

2.3.3 Geometric Parameter Tests

Now it is important to focus on the actual parameters that were considered in this study. Fin height variation was the first geometric parameter to be studied. A summarization of the test conditions are listed below:

- $3mm \leq h \leq 50mm$
- L = W = 75mm
- $k=k_{Al}$ (150-280 W/m-k)

Figure (2.5) below is a graph of the experimentally determined thermal resistance versus the number of fins for various fin heights as found by Bibir and Fijols [3]. For this experimental study, each of the five curves was prescribed a constant fin thickness of .8mm over a length of 75mm. Holding the length constant while varying the number of fins means that the fin spacing and wetted surface area varies [3].

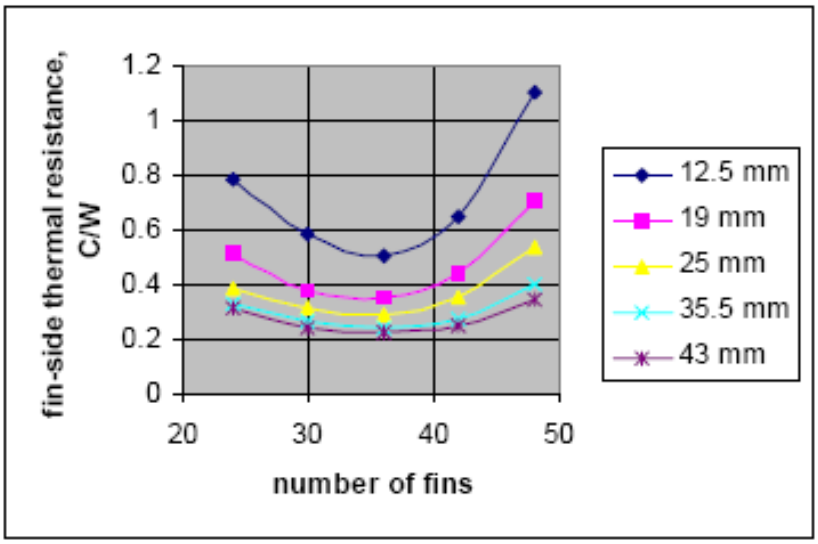

Figure 2.5: Thermal Resistance vs. Number of Fins for Varying Fin Heights

Physical interpretation of this study shows that as the number of fins decreases, the gap between the fins increases. It can be seen from Figure (2.5) that for each of the fin heights with forced convection, the highest thermal resistance values occur at both low and high number of fins. The ideal number of fins for all of the curves is found at the middle of each curve, which can be estimated around 35-36 fins (~2fins/mm).

These results show that having a small number of fins with large gap spacing between them is not optimal. It's ideal to keep the surface area as high as possible, as $q = hA_w(T - T_\infty)$.

Low fin performance also occurs when using a high number of fins. As aforementioned, as the number of fins increases over a fixed heat sink length, the gap spacing between adjacent fins decreases. This result shows that there is simply not enough space for free air to move through the fins to create good performance (Figure 2.6).

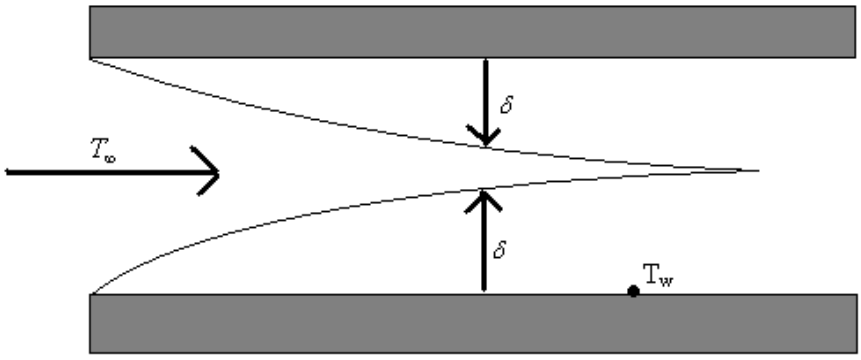

Figure 2.6: Converging Boundary Layer Sketch [4]

This is because T_{air} increases to values greater than T_{∞} in the free stream when the adjacent boundary layers merge, which consequently outweighs any value of added fin surface area.

From all of this, a handful of conclusions can be made regarding the results. Firstly, the variation in thermal resistance drastically decreases as the height of the fins increases. For example, take a look at the diamond (blue) curve which denotes a fin height of 12.5mm. The thermal resistance varies from roughly .5-1.15 k/W, whereas the star (purple) curve which denotes a fin height of 43mm has a resistance range between .2-.35. Simply put, if the height of the fins is increased to a maximum, changing the total number of fins results in a smaller change in total resistance value.

Secondly, the overall fin effectiveness versus fin height can be discussed. The curves above show that as the fin height increases, the rate at which the fin performance increases begins to decrease. For example, the difference in overall fin performance for fin heights of 12.5mm and 19mm is quite large, which can be seen from the large difference between them on the graph. By comparison, the overall thermal resistances decreases as the fin height increases from 25mm to 43mm, but only by a relatively small amount. Cost factors may lead manufacturers to use the 25mm fin height as the improvement in effectiveness becomes negligible at larger heights.

The second parameter that was tested is the base thickness of the heat sink. But first, the definition of total and spreading resistance should be briefly mentioned [5].

The total resistance of the system is equal to the fin-side resistance plus the spreading resistance. In relation to the copper spreader test that will be presented later in this paper, the spreading resistance here would parallel the resistance the copper base plate produced.

Consequently, Figure 2.7 shows that the change in number of fins has only a small affect on the value of the spreading resistance. Therefore, finding an optimal geometric design to minimize thermal resistance of a heat sink without the presence of fins has been validated. Adding fins will only further optimize the entire system. Finally, Figure 2.7 shows that the fin resistance and total resistance show gradual decreases in value as the number of fins increases.

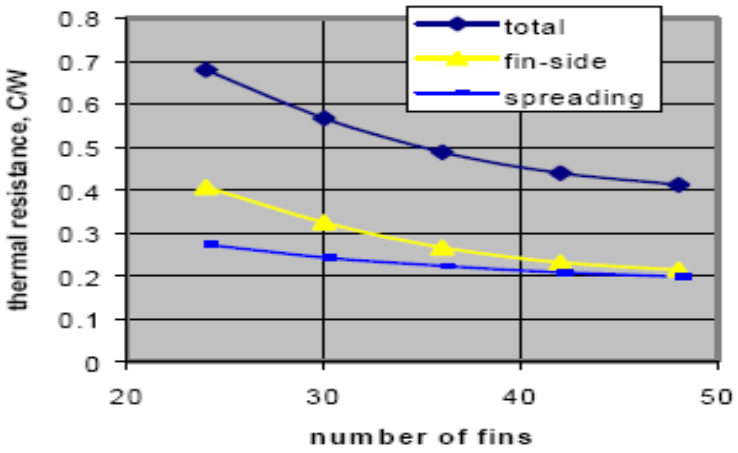

Figure 2.7: Thermal Resistance Components for Spreading & Fin Side Resistance [3]

The effect of base plate thickness was studied next. For this study, the height of the fins was held constant at 50mm, and the thickness of the fins was held at .3mm. The results for a changing base plate thickness with number of fins are shown in Figure 2.8 [3]:

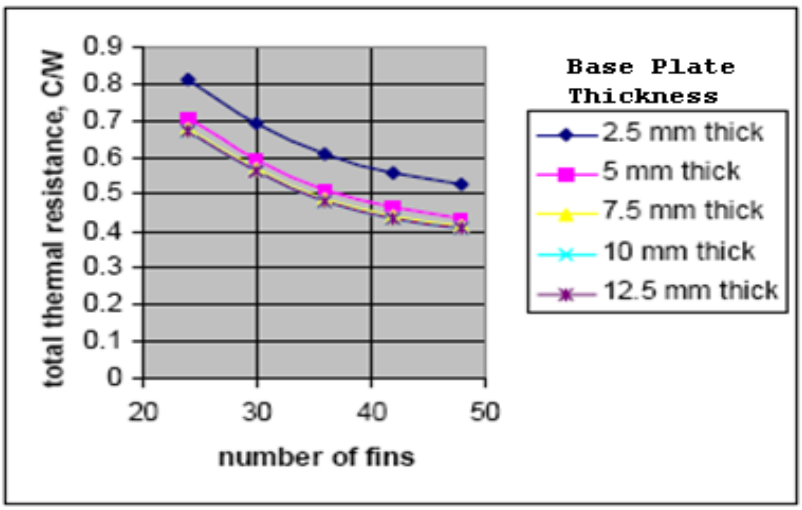

Figure 2.8: Thermal Resistance vs. Number of Fins for Varying Base Plate Thickness

This shows that various base plate thicknesses have an effect on the total resistance for all fin densities. The most important conclusion is that there is only a small performance increase for any base plate thickness larger than 7.5mm.

The last parameter that was tested in this study involved fin thickness. For this test, the height of the fins was held constant at 43mm. Figure 2.9 shows the direct effect of number of fins on the performance of the heat sink. This is a powerful result which ultimately shows how fin thickness and spacing affect heat sink performance [3].

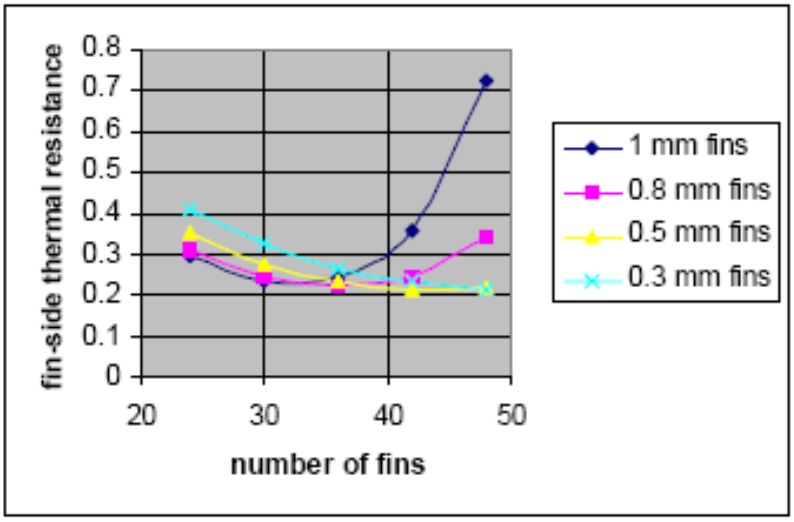

Figure 2.9: Thermal Resistance vs. Number of Fins for Varying Fin Thickness

Table 2.3 summarizes the test parameters for the .3mm, .5mm, and .8mm thick fins:

Table 2.3: Fin Packs Shown for Figure 2.8 Above

Fin Thickness[mm]	**# of Fins**	**Max # of Fins (75mm Flow Width)**
.3	48	62
.5	42	38
.8	36	24

Figure 2.9 clearly shows that the 1mm thick fin for the case of a large number of fins can almost be completely disregarded right away. The resistance increases rapidly once more

than 38 fins are used. The results for the other three fin thicknesses are more similar. An optimal decision seems to be this: increase the number of fins, and make them as thin as possible to achieve the most efficient fin design. Therefore a fin of .3mm thickness, which allows a maximum of 48 fins, appears the most ideal.

2.3.4 Recap of the Results

After thoroughly analyzing and interpreting the results individually, a few final conclusions can be drawn from the analysis in this section. Total thermal resistance is lowered as the number of fins increases, which is expected. In addition, a thick copper base plate 5mm-7.5mm thick can be used to lower the overall thermal resistance, where having a thicker base plate does not increase the effectiveness.

The results of greatest importance were those showing the performance as a function of varying fin height and thickness. The thinner the fin, combined with a greater number, creates the most ideal design. In contrast, the results of varying fin heights with either small or large numbers of fins results in a non-ideal thermal outcome. It appears that the optimal design occurs for a base thickness of 7.5mm, with thin fins ranging from .3mm-.5mm, and a fin height of 30mm. Table (2.2) relates the fin thickness to minimum gap spacing for a set spreader width. In addition, an intermediate number of fins are ideal. Too few fins, and there isn't enough surface area to lower the thermal resistance. Too many fins, and air cannot effectively flow through the fins. For this reason, the optimal value in this study was found to be roughly around 40 long thin fins. This is because the test was run with a fixed width, and this number of fins results in optimal fin spacing. This gives the large perimeter

to area ratio necessary to increase the overall efficiency and performance of the fins added to the heat sink (shown in equations 2.22 and 2.23). This geometry also gives a corresponding low resistance.

CHAPTER 3

Experimental Study of Heat Sink

3.1 Experimental Explanation

3.1.1 Phases

This portion of the paper focuses on the experimental study and analysis of a high performance heat sink. Due to the extensive length of this study, the discussion for this experiment will be broken down into different phases. These experimental phases include the study of heating one heat sink with free convection at four different output power settings, calibrating and normalizing each of the heat sinks used, finding temperature dependant air properties, forced convection tests at six different air speeds for one heat sink inside an insulated wind tunnel, and finally a second forced convection test for two heat sinks in tandem at various gap spacings and air speeds.

3.1.2 Goals

There are numerous goals and conclusions to be drawn from this study. The first study for one heat sink being cooled by free convection yields the ability to test the performance of the heat sink and compare these measurements to the power vs. temperature curve that the Wakefield Engineering Company provided for the device. This process of

comparing our experimental results against the company results is a way to verify that the testing procedure used here is consistent with that of the manufacturer.

Secondly, it was important determine the consistency of our measurements. Each of the two heat sinks had the same size heater pad mounted to the bottom of the device, and was tested. It was found that a difference in tightness of the brackets that held the heater pads in place produced a slight difference in performance. By running both of the heat sinks at the same conditions, the average difference in performance was determined. Next, because the forced convection performance experiment involved the heat sinks at various air speeds, the steady-state maximum heat sink temperature varied for each test. Therefore, correlations were found for all of the air properties as a function of temperature. These properties included density, prandtl number, kinematic viscosity, dynamic viscosity, etc…

After the free convection portion of this experiment was completed, a forced convection study was conducted on a single heat sink. By analyzing the maximum temperature of the device, along with the average air speeds, an experimental Nusselt number correlation was obtained which can be used to determine the convection coefficient for any other test scenario for this heat sink. Similarly, by analyzing two heat sinks in tandem inside a wind tunnel, a second Nusselt number correlation can be found for this particular test situation.

3.1.3 Experimental Setup & Devices

Before the results from the experiment can be discussed, it is important to briefly mention all of the devices that were used for the heat sink study. An Omega OMB-DAQ56

data acquisition device (DAQ) was used, which allowed for ten different thermocouple temperature readings to be acquired and stored at equal time intervals (Figure 3.1).

Figure 3.1: DAQ Device Containing 10 Thermocouple Attachments

This device has software that automatically inputs every temperature reading directly into Microsoft Excel® at user defined time increments. Throughout every phase of this experiment, this device was used to acquire all of the temperature measurements. The high performance heat sinks used in this study is shown in Figure 3.2 below:

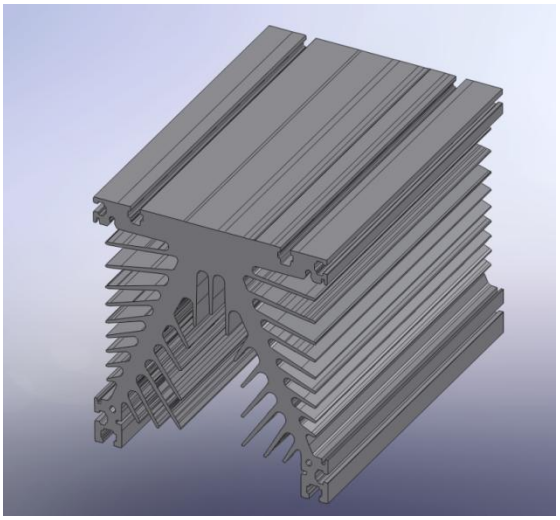

Figure 3.2: 392-180 High Performance Wakefield Engineering Heat Sink

A 3” by 5” silicon heating pad (Model Number: Omega SRFG-305/10-P) was placed in between two aluminum plates of identical dimensions, and this heater assembly was mounted to the heat sink, thus producing a constant temperature distribution over the entire size of the heater. The placement of the heater assembly is shown below in Figure 3.3:

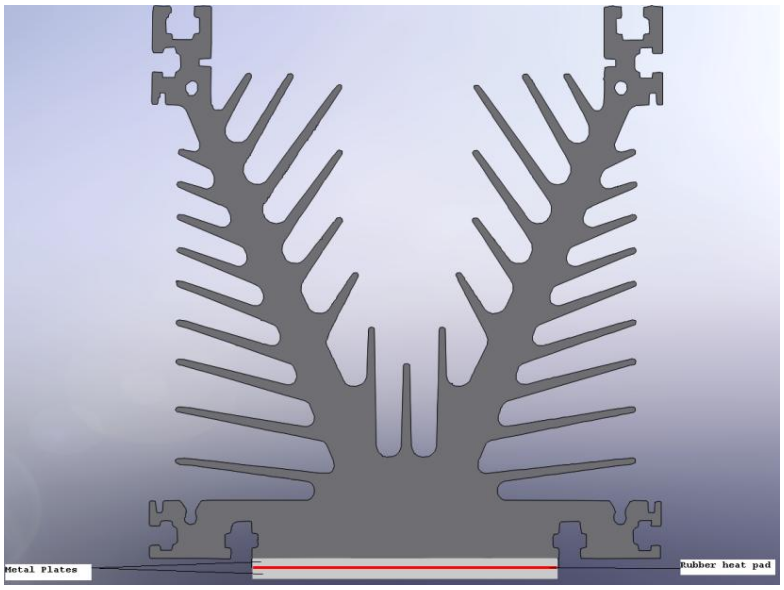

Figure 3.3: Testing Orientation with Heater Pad Location, Front View

By placing insulation over the entire bottom face of the heat sink and heater assembly during all tests, all heat generated passes through the heat sink. Variac’s were used to control the amount of power to the heaters (Figure 3.4). This device takes power from any regular wall outlet, and using the dial, any voltage setting up to 130 volts can be input to the heaters. By knowing the heater pad resistance and desired heater power, the value for the heater voltage

can be easily obtained using $V = \sqrt{PR}$. Voltage or resistance readings were found using a handheld multimeter:

Figure 3.4: Variac Power Supply

Finally, two different devices were used to find the air speed inside the wind tunnel. A hot wire velocimeter is a device used to find velocities at one specific point, and was generally used to find velocities upstream of the fins of the heat sink.

The second device is a propeller anemometer, and yields an average velocity over the propeller capture area. The propeller anemometer is shown below in Figure 3.5. This device was placed at the outlet of the wind tunnel duct, and was used to set the experimental wind tunnel air speed.

Figure 3.5: Propeller Anemometer

3.2 Calibration

3.2.1 Purpose

Comparison tests were first conducted to determine how sensitive measurements are to variations in setup. The purpose of conducting such a test is because it is impossible to set up the heat sinks exactly the same. Therefore, a free convection test was run to compare two heat sinks each with their own heater, assembly, and insulation.

Each of the heat sinks were placed in a room on a table at a considerable distance from one another, so that the heat generated wouldn't affect the surrounding ambient temperature. It was assumed that the ambient temperature of the entire room is constant over the testing period.

3.2.2 Tabulated Results

For this test each of the heat sinks was tested at four different heater power settings: 60, 80, 100, and 120 watts. The power output can easily be set using the basic equations shown below [5]:

$$\text{P(watts)} = \frac{V^2(volts)}{R(\Omega)} \tag{3.1}$$

$$V = \sqrt{P\,R} \tag{3.2}$$

This was important to set each heater voltage independently because each of the two heater pads had slightly different resistance values. Heat sink one (HS_1) and heat sink two (HS_2) carried heater pads with a resistance of 86 and 92.5 ohms respectively. Each of the four tests were conducted once, and then the test scenario was repeated after thermal grease had been placed in between the aluminum heater plates and the heat sink itself. Thermal grease is used to overcome surface imperfections and to minimize the thermal contact resistance between the heater and the heat sink [6]. An example of the data generated from this test is shown below in Table 3.1:

Table 3.1: Results for Free-Convection Calibration with Thermal Grease

			front hs	back hs			
Power (W)	**V_1**	**V_2**	**$T_{max, HS1}$**	**$T_{max, HS2}$**	**$\Delta T_{, HS1}$**	**$\Delta T_{, HS2}$**	**$\Delta T_{, HS1}$-$\Delta T_{, HS2}$**
60	71.83	74.50	57.528	55.662	33.383	31.516	1.867
80	82.95	86.02	67.321	65.878	43.675	42.232	1.443
100	92.74	96.18	76.817	75.646	53.167	51.996	1.171
120	101.59	105.36	88.414	85.894	64.211	61.691	2.520

It can be seen that by setting the experimental power values in the first column, Equations (3.1) and (3.2) can be used to calculate the voltages required for each of the two heat sinks. Experimental voltages required were read using a digital multimeter. The last column gives the difference in temperature difference $\Delta T_{Hs,i} = (T_{max,i} - T_{\infty,i})$ between the two heat sinks. It was found that the first heat sink was between 1.5-2.5 degrees hotter than the second heat sink. It is believed that this is due to the slight difference in mounting the heater assembly.

In addition, a simple heat transfer calculation can be used to find the overall thermal resistance of each device [7]:

$$R_{thermal} = \frac{\Delta T_{\max}}{P} \tag{3.3}$$

The results corresponding to Table 3.1, are shown in the Table 3.2 below:

Table 3.2: Results of Free-Convection Calibration Test with Thermal Grease

$\mathbf{ThermRes_{HS1}}$ [ºC/Watt]	$\mathbf{ThermRes_{HS2}}$ [ºC/Watt]	ΔThermRes [ºC/Watt]	% Error
0.556	0.525	0.031	5.592
0.546	0.528	0.018	3.304
0.532	0.520	0.012	2.202
0.535	0.514	0.021	3.924

As shown in the above table, the first heat sink has a thermal resistance value ~ .02K/W higher, on average, than the second heat sink. By normalizing these two devices, the .02 difference will have to be taken into account when the forced convection tests are conducted later in the experiment.

3.2.3 Graphical Results

For a free convection heat sink, it is also on interest to know how the maximum temperature values are related to the heater powers. By looking at Equation (3.3), the relationship should be linear. The measured results are shown graphically in Figure 3.6:

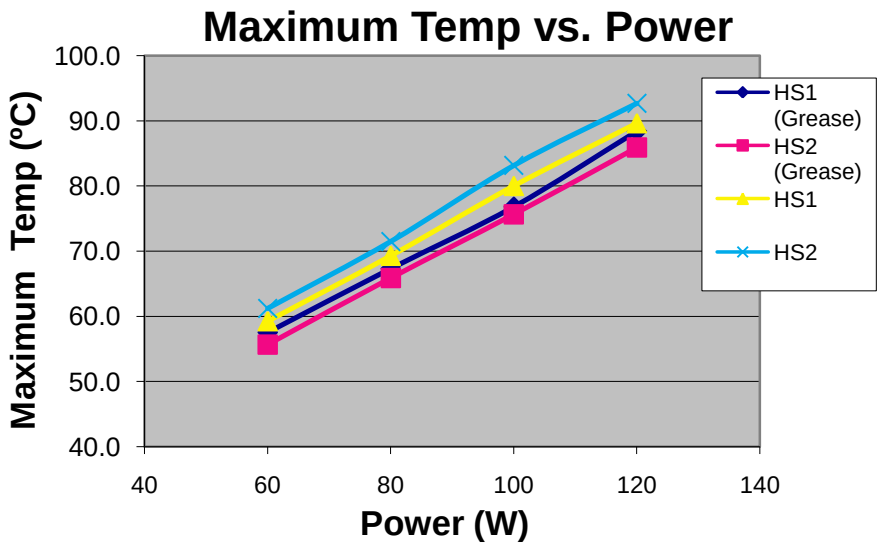

Figure 3.6: T_{max} vs. Power Curve for Free-Convection Calibration Test

Whether the test was run with or without thermal grease, the maximum temperature, which is located anywhere on the aluminum plates due to the insulation around the heater (this is where the thermocouple was placed), does indeed increase linearly with the heater power. The two lower curves generated are the tests ran with thermal grease, and it can be seen that the maximum temperature values are slightly lower than those for the case without thermal grease. This validates that thermal grease does indeed positively affect the overall performance of the heat sink. In addition, the heat sink maximum temperature never exceeds 95 degrees Celsius for heater powers less than 120 watts.

It is also important to look at the relationship of the thermal resistance relative to the heater power. By using the temperature and power measurements above to create the thermal resistance curve, as shown in Figure 3.7, validates for a second time that thermal grease lowers the overall thermal resistance.

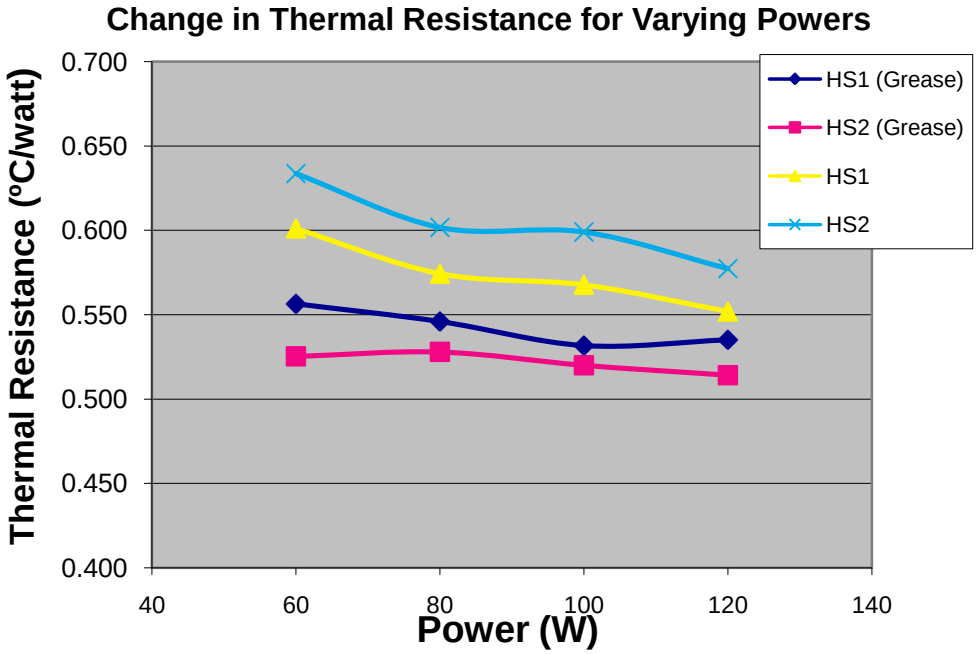

Figure 3.7: R_{max} vs. Power Curve for Free-Convection Calibration Test

Finally, by looking at Table (3.2) and Figure (3.7), it can be stated that the maximum overall thermal resistance never exceeds .6ºC/W (with thermal grease). This is an important value to keep in mind because the forced convection tests will ultimately yield lower overall thermal resistance values. Therefore, these results are a worst possible scenario for the high performance heat sinks being analyzed.

3.2.4 Experimental Error

As an aside, failing to carry out this comparison test was a potential source of error in this experiment. The first time all of the forced convection tests were carried out, neither of the devices had thermal grease applied to the contact region. As well, the calibration test itself had not been carried out; therefore producing skewed results that were difficult to explain. Because of this oversight, the two heat sinks were then compared, and the forced convection tests were repeated after normalization had been completed.

3.3 Free-Convection Test

The next portion of this experiment considered a free-convection test with one of the heat sinks for the purpose of comparing our measured overall performance results with published ones from Wakefield Engineering.

The design scenario ran was similar to the calibration test, except the test included two parameters; with and without bottom insulation. Four different voltage values were chosen and input to the resistance heater of one heat sink. The device was then allowed to reach a steady-state temperature. A curve of the temperature verses time is shown in Figure (3.8) below:

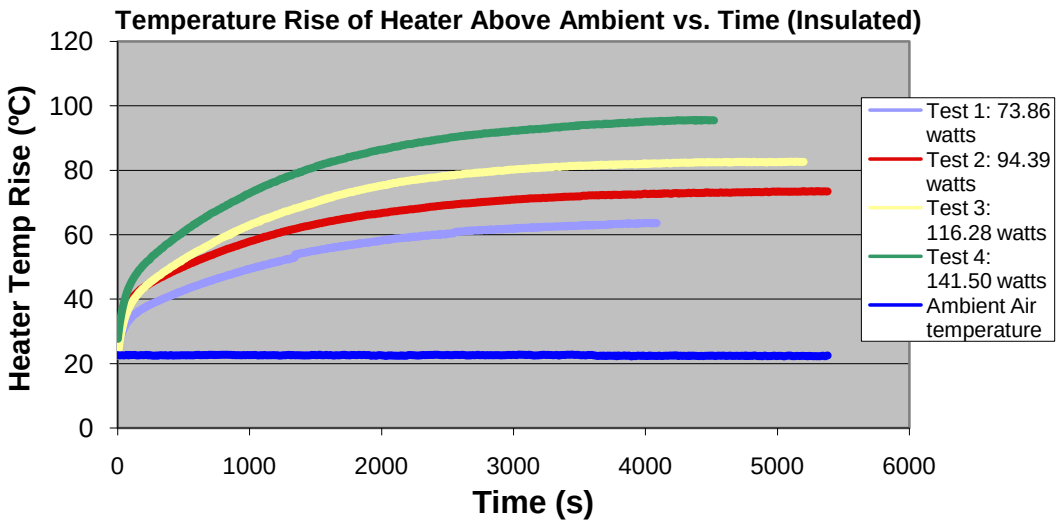

Figure 3.8: Temperature vs. Time Curve for Free-Convection Test

It reveals that the majority of the temperature increase occurs prior to 2000 seconds (33 minutes), whereas at longer times the overall maximum temperature increases only marginally. Similar to the calibration test, the maximum temperature value doesn't exceed 95ºC when Power ≤150 watts.

The main purpose of this study is to compare the experimental results to the results provided by the Wakefield Engineering Company. The results are shown below in Figure 3.9:

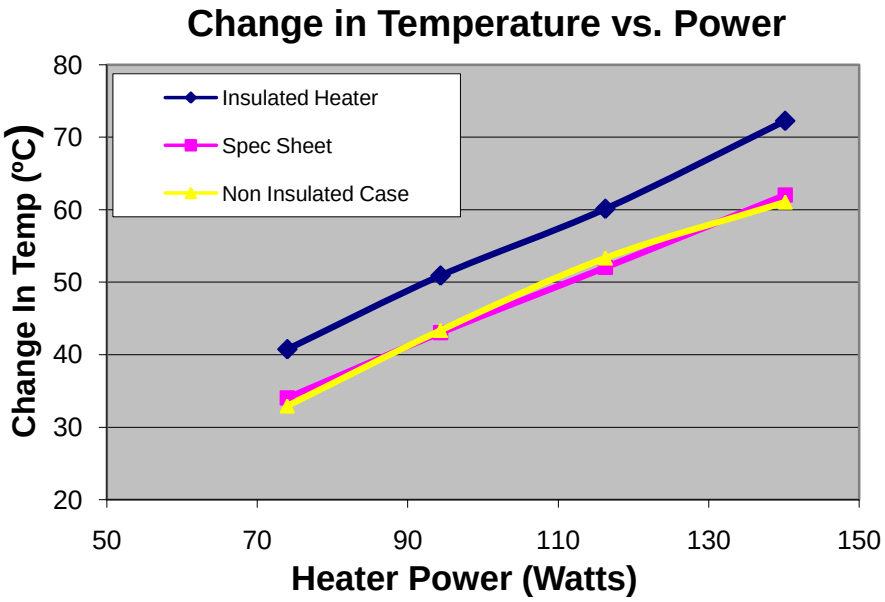

Figure 3.9: ΔT_{max} vs. Power for Free-Convection

As aforementioned, the insulation forces all the heat from the heater to flow into the heat sink. Because of this, the maximum temperature is, and should be higher for the insulated case compared with the non-insulated case. Furthermore, it was found that the non-insulated results yielded nearly identical results to the values given by Wakefield. This simple test confirms that our experimental technique is correct.

3.4 Air Property Correlations

In order to obtain an experimental Nusselt number correlation, all known heat transfer parameters must be calculated. Yet, all of these parameters have changing values dependent on the temperature. An example of two air properties parameters is shown in Table 3.3 below [8]:

Table 3.3: Temperature Dependant Heat Transfer Parameters [8]

Temp [°C]	Temp [K]	Therm. Cond (k) [W/m-K]	Prandtl #
0	273.15	0.0243	0.715
20	293.15	0.0257	0.713
40	313.15	0.0271	0.711
60	333.15	0.0285	0.709
80	353.15	0.0299	0.708
100	373.15	0.0314	0.703
120	393.15	0.0328	0.7
140	413.15	0.0343	0.695
160	433.15	0.0358	0.69
180	453.15	0.0372	0.69
200	473.15	0.0386	0.685

Because this experiment covers a wide range of steady-state temperatures, best fit correlations were produced for every air property needed (Figure 3.10). Below is an example of two of the air properties [8] along with corresponding best fit curves:

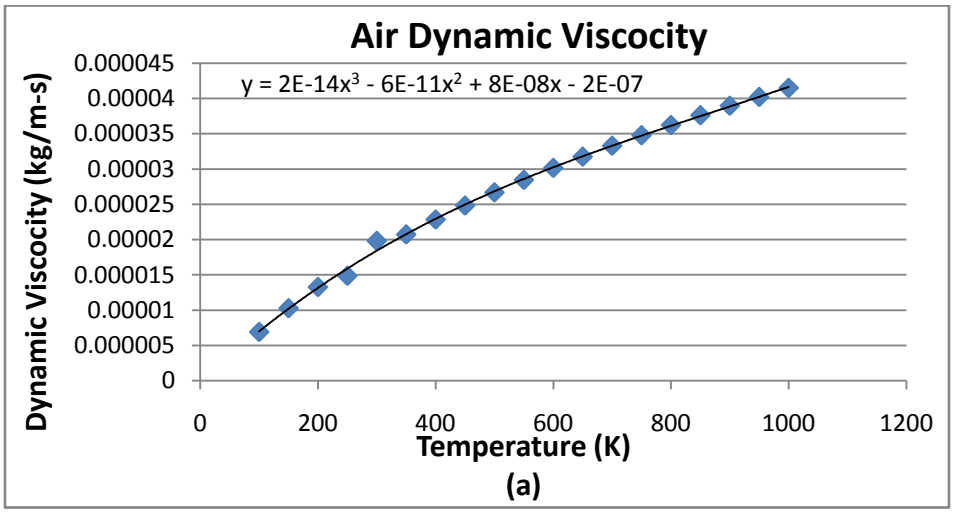

Figure 3.10a: Dynamic Viscosity Correlation

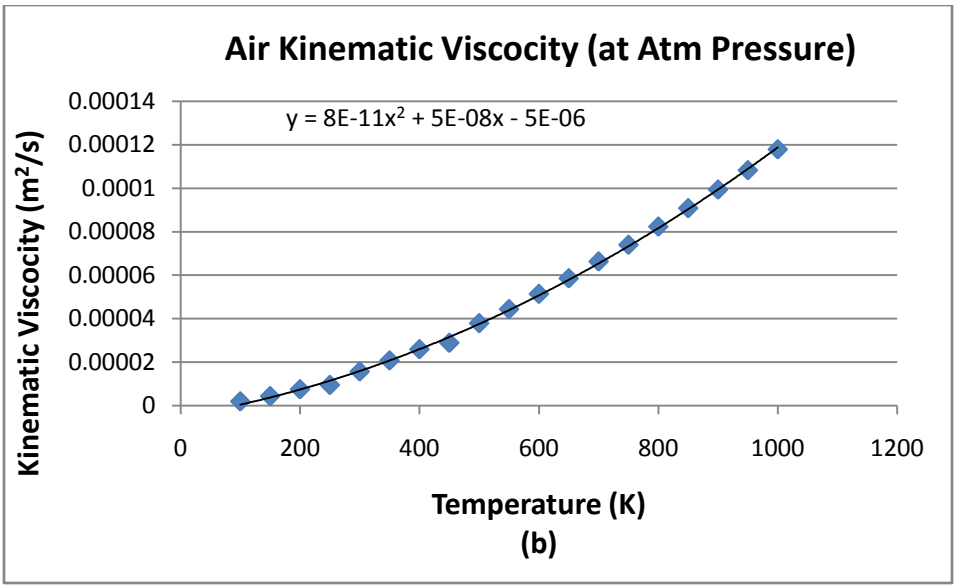

Figure 3.10b Kinematic Viscosity Correlation

All of the temperature (in Kelvin) dependent air property correlations are given below:

Dynamic viscosity, (3.4)

$$\mu = 2x10^{-14}(T^3) - 6x10^{-11}(T^2) + 8x10^{-08}(T) - 2x10^{-7} \text{ [kg/m-s]}$$

Kinematic Viscosity, (3.5)

$$\nu = 8x10^{-11}(T^2) + 5x10^{-8}(T) - 5x10^{-6} \text{ [m}^2\text{/s]}$$

Thermal Conductivity, (3.6)

$$k = 7x10^{-5}(T) + .0046 \text{ [W/m-K]}$$

Prandtl Number, (3.7)

$$Pr = -3x10^{-7}(T^2) + 8x10^{-5}(T) + .7166$$

For simplicity, the value for the density of air is assumed to be constant. This assumption is made because the range of the density values was minimal within the range of experimental steady-state temperature values (50ºC-100ºC). These air property correlations will be used

extensively in the next two sections where the forced-convection experiments are presented. Once the experimental maximum temperature values have been found with the DAQ device, equation's (3.4)-(3.7) will be used to calculate experimental Reynolds number, and ultimately Nusselt number.

3.5 One Heat Sink: Experimental Setup and Results

3.5.1 Forced Convection Experimental Setup, One-Heat Sink

Now that the foundation of the experiment has been laid out, the main part of the experiment can be discussed.

Before the results are presented, photographs of the experimental setup and a brief description will be given. For the forced-convection experiment with one heat sink inside the insulated wooden duct, a propeller anemometer was used to set up the wind tunnel air speed. The location of the anemometer is shown in the Figure 3.11 below:

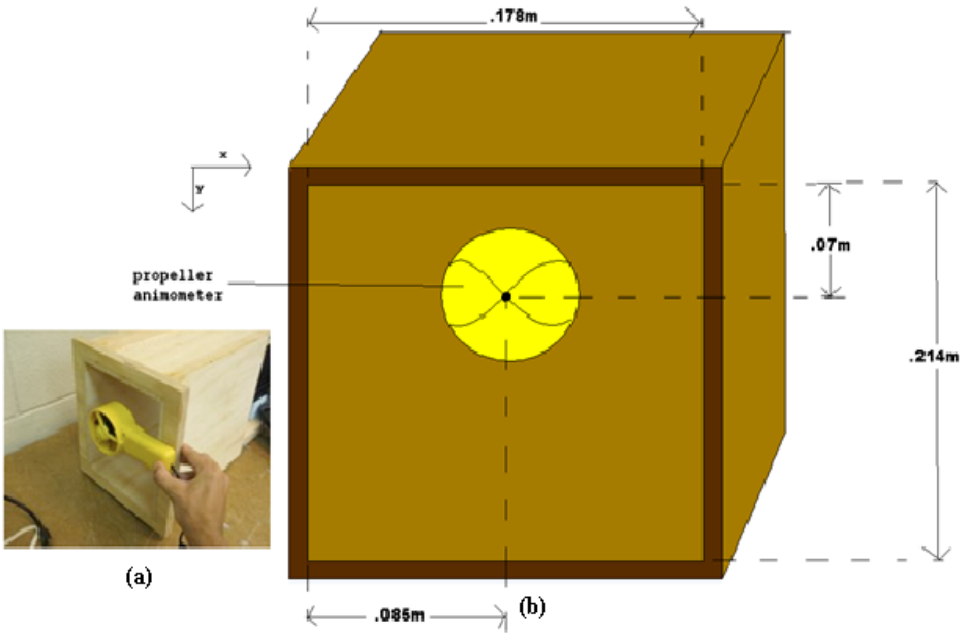

Figure 3.11: (a) Actual Anemometer Location at Duct Exit, (b) Sketch of Duct Exit With Dimensions

Figure 3.11(a) shows where the anemometer was placed during all forced convection tests. The picture on the right was generated in order to give an idea of the relative size of the duct and propeller. Figure 3.12 shows the wooden duct and the location where the heat sinks were placed for the forced convection tests:

Figure 3.12: (a) Outside View of Wooden Duct, (b) End View into Duct

It can be seen that the heat sinks were precisely centered inside the duct, to create symmetric airflow on the left and right sides of the heat sink. Analyzing the photo on the left, the generated air flows from right to left through the duct. Looking at Figure 3.12b, flow comes out of the page.

3.5.2 Known Experimental Parameters

For this experiment, there are many geometric parameters that are necessary in order to analyze the temperature results. These parameters are constant throughout the entire forced-convection tests, and are summarized in Table 3.4:

Table 3.4: Table of Known Parameters

Given Power for Heat Sink	$q_{conv,\ fin}$=	150	watts
Wetted Area of Heat Sink	A_{wetted}=	0.4163	m^2
Heat Sink Length	L_c=	0.18	m
Duct Cross Sectional Area	$A_{c,\ duct}$=	0.03809	m^2
Flow Area of Air	A_c=	0.02595	m^2
Heat Sink Perimeter	P =	3.119	m
Flow Hydraulic Diameter	d_h=	0.0333	m

- Where $q_{conv,\ fin}$ is the set power the variac produces on the heater (150W for these tests).
- Where A_{wetted} is the surface area of the heat sink exposed to the air flow (i.e. every surface but the bottom face that the insulation covers.
- Where L_c is the length (in flow direction) of the heat sink.
- Where $A_{c,\ duct}$ is the cross sectional area of the duct.
- Where A_c is cross sectional flow area [$A_c = A_{c,duct} - (A_{c,HS} + A_{c,\ insulation})$]
- Where **P** is the wetted perimeter of the front face of the heat sink, the duct, the foam
- Where d_h is the hydraulic diameter of the system

A few of these components were not able to be calculated by hand; therefore alternative methods were used to find their values. For instance, it was not feasible to find the wetted surface area of the heat sink by hand. Therefore, the front face of the actual heat sink was scanned into a photo processing program. Then, this file was manually converted and scaled into SolidWorks®. From this, SolidWorks® has a function that gives the cross sectional area

and perimeter of the front face of the heat sink. Having this knowledge, and understanding that the wooden duct and styrofoam insulation both have rectangular cross-sections; all other parameters could be calculated by hand. Furthermore, from this scanned image, the two-dimensional image was extruded the full length of 180mm to generate the device shown in Figure (3.2). Finally, the hydraulic diameter can be calculated by the simple equation [9]:

$$d_h = \frac{4A_c}{P} \tag{3.8}$$

3.5.3 Thermocouple Locations

For the forced-convection experiments for one heat sink, six different thermocouples were used. The locations of these thermocouples are shown in Figure 3.13 below:

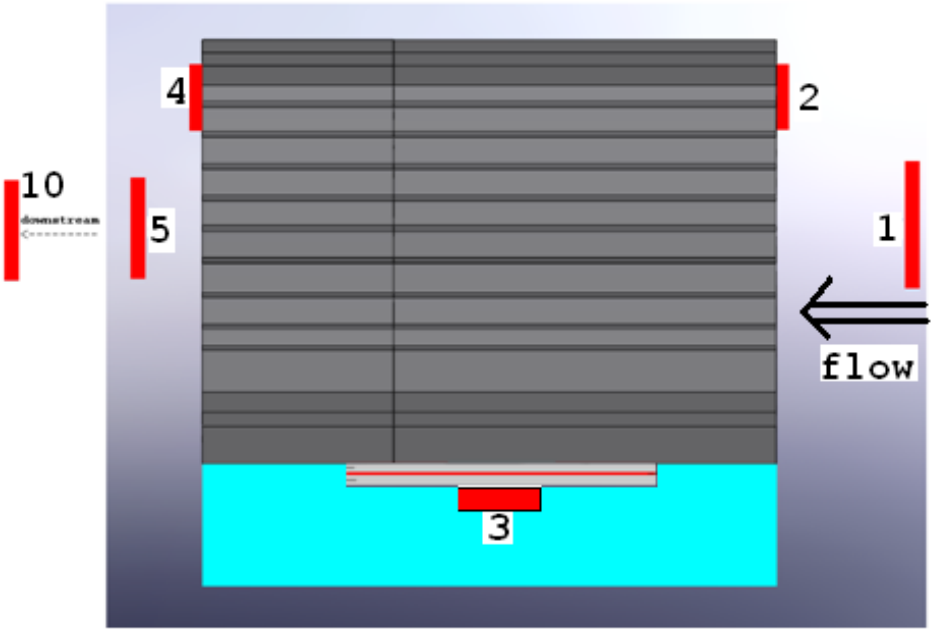

Figure 3.13: Thermocouple Locations for One Heat Sink Forced Convection Test

For this experiment, thermocouple one measures the upstream ambient air temperature (T_∞) for this heat sink. Thermocouple three is placed directly onto the bottom of the aluminum plate of the heater assembly. Because the heater is insulated on the bottom side, T_3 is considered the maximum temperature in the system, i.e. $T_3=T_{max}$. Thermocouple ten was placed at the duct exit, primarily to measure if there was any temperature difference between the upstream and downstream ambient air temperatures.

3.5.4 Thermal Results

As mentioned earlier, all test conditions were set based on the average outlet duct velocity, measured using the propeller anemometer in increments of 1,2,3,…,6m/s. Each of the six tests was allowed to reach a steady state temperature. The results are shown in Table 3.5 below:

Table 3.5: Results from Forced-Convection Test: One Heat Sink

	T_3	T_3-T_1		
$V_{outlet,\ avg}$ (m/s)	**T_{max} (ºC)**	**$\Delta T_{max}(T_{max}-T_{upstream})$ (ºC)**	**R_{th} (ºC/W)**	**h_{HS1} (W/m^2-ºC)**
1.000	82.250	57.776	0.385	6.237
2.000	68.900	44.713	0.298	8.059
3.000	62.120	37.751	0.252	9.545
4.000	59.210	34.993	0.233	10.297
5.000	57.890	33.479	0.223	10.763
6.000	56.25	32.418	0.216	11.115

From this data, a few summary points can be made. Firstly, the maximum temperature for the six cases was 82.25°C, where the largest change in temperature, ΔT_{max} was 57.776°C. As

shown earlier in Table 3.2, the overall thermal resistance for the heat sink in a natural convection environment was .514<R_{free_conv} <.556 ºC /Watt. By comparison, the range of thermal resistance values due to forced convection was .216<R_{forced_conv} <.385ºC/Watt.

Even at the lowest fan speed, the overall efficiency of the heat sink is roughly 35% higher than the free-convection case. By simply comparing these values, the benefits from even small forced convection are rather large. Blowing air with some type of small fan is recommended over using natural convection.

3.5.5 Analyzing the Results

Next, we examine the maximum temperatures in more detail. Plotting maximum temperature verses air velocity, it can easily be seen that as the velocity of the air increases, the maximum heat sink (Figure 3.14) temperature decreases.

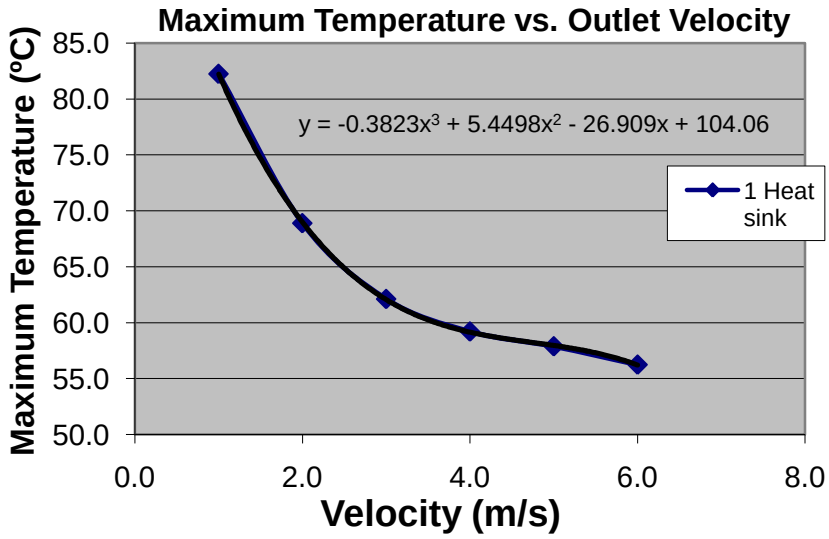

Figure 3.14: Max Heat Sink Temp vs. Outlet Air Velocity

The results show a considerable drop in maximum heat sink temperature from the lowest air speed up to 3 m/s. Whereas, the maximum temperature of the heat sink levels off, and does not vary much when air speed is 4 m/s, 5 m/s, or 6 m/s. A few conclusions can be drawn from this. An average air speed of 3 m/s seems to be a reasonible air speed to have flowing over this heat sink to yield an efficient system, as the maximum temperature for this test is <65ºC. Although higher fan speeds produce a lower overall thermal resistance (Figure 3.15), this positive may not outweigh other factors such as increased running cost and noise level from the fan.

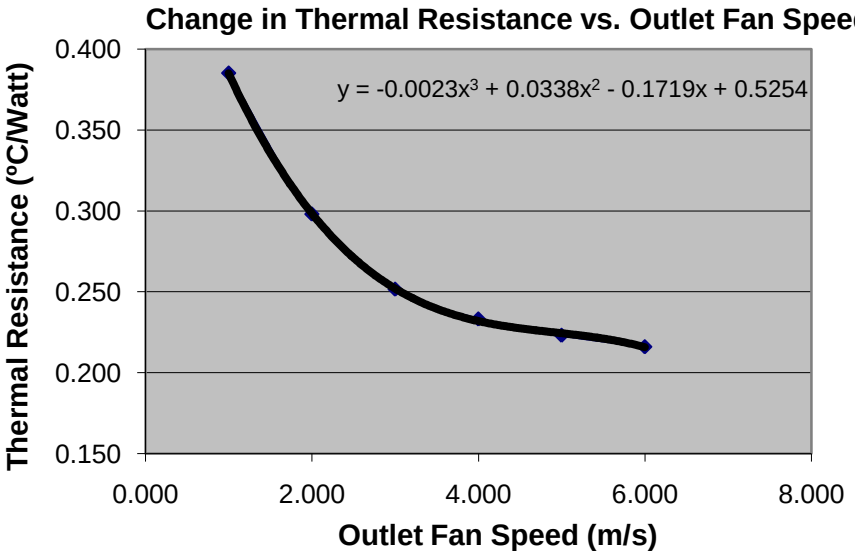

Figure 3.15: Thermal Resistance vs. Outlet Fan Speed

Convection coefficient values (h) were calculated using the equation below [2]:

$$h_{exp} = \frac{q_{conv,fin}}{A_{wetted}(T_{base} - T_{\infty})} \tag{3.9}$$

In this equation, the base temperature coincides with the maximum temperature of the heat sink (T_3), and T_∞ is the ambient air temperature, or T_1. Experimentally determined values for h are given in Table 3.5 above. Equation (3.3) for fixed power shows that maximum temperature and thermal resistance have a linear relationship. Therefore, the thermal resistance shown in Figure 3.15 should yield the same shape as the maximum temperature curve shown in Figure 3.14.

The Biot number is a ratio of the conduction resistance in the heat sink to convection resistance. It is calculated by:

- $Bi = \frac{hl}{k_{air}}, where\ l = \frac{Volume}{A_w}$

If the Biot number <.1, then the temperature gradients within the heat sink can be neglected. Figure 3.16 shows that the Biot number is well above .1 for all air flow velocities.

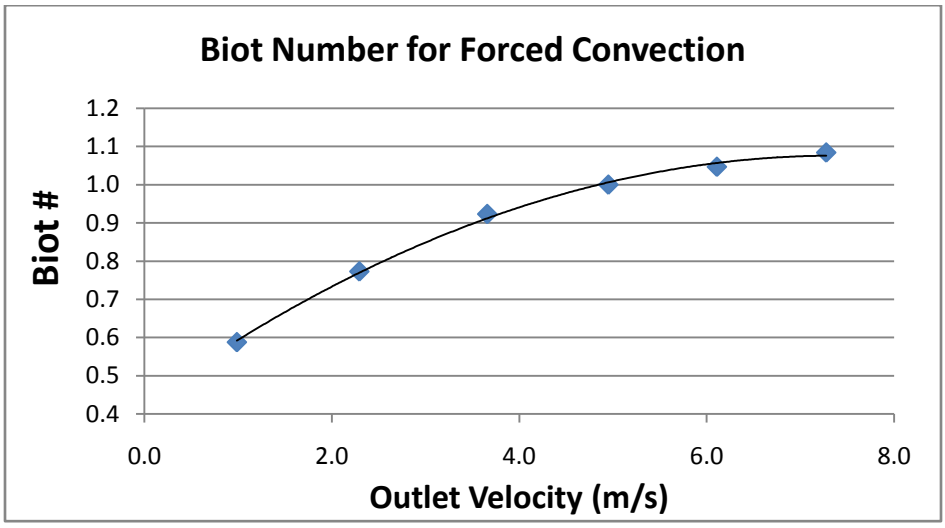

Figure 3.16: Biot Number for Forced Convection Test

The higher the Biot number, the larger the temperature difference between the base (T_3=T_{max}) and the tip of the heat sink (T_2, T_4). Table 3.6 below shows the temperature readings taken with the DAQ device every ten seconds, after steady state has bee reached. It can be seen that T_3 is nearly 30ºC hotter than T_2 or T_4.

Table 3.6: Sample of DAQ Steady State Temperature Results at 3 m/s

Test 3:	**3 m/s**				
Sensor 1 (ºC)	**Sensor 2 (ºC)**	**Sensor 3 (ºC)**	**Sensor 4 (ºC)**	**Sensor 5 (ºC)**	**Sensor 10 (ºC)**
24.311	32.706	62.157	32.135	25.606	25.550
24.254	32.718	62.114	32.095	25.551	25.529
24.347	32.801	62.212	32.170	25.501	25.509
24.373	32.795	62.207	32.195	25.546	25.386
24.397	32.800	62.139	32.080	25.584	25.371
24.373	**32.724**	**62.124**	**32.102**	25.491	25.378

3.5.6 Analysis of Temperature Time Constant

Finally, the last parameter that will be briefly discussed is the thermal time constant, denoted by the Greek letter τ. Physically, the thermal time constant is the time it takes the system to reach 63.2% of its final asymptotic maximum temperature value. In our case, the time constants were found for T_2 and T_3, as shown in Figure (3.13). By finding these time constants, they can indicate how rapidly this device will exponentially increase or decrease in temperature. To find the time constants, the data from the DAQ device was used, where time and temperature readings for both thermocouples were tabulated in ten second increments. To find the time constants, $\theta(t)$ had to be found by:

$$\theta(t) = \frac{T(t) - T_{\max}}{T_i - T_{\max}} \tag{3.10}$$

Where graphs of *–ln[$\theta(t)$] vs. time* for all six outlet speeds for T_2 and T_3 were produced. These graphs will produce a linear relationship, where the 1/slope is considered the time constant. Results can prove to be rather accurate within a 5% error. The results are shown below in the Table 3.7 and are also plotted in Figure 3.17 below:

Table 3.7: Temperature Time Constant for Wakefield Heat Sink

Outlet Velocity (m/s)	$\tau_2(s)$	$\tau_3(s)$
1	715	714
2	690	476
3	345	333
4	313	278
5	303	200
6	250	196

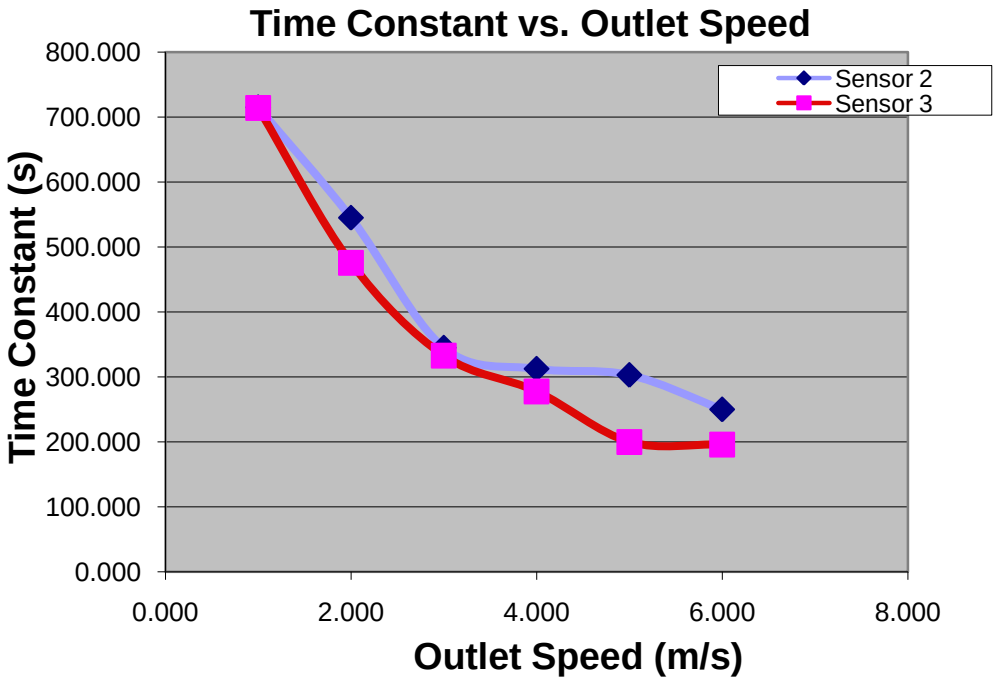

Figure 3.17: Time Constant for Various Outlet Speeds

Viewing the table and figure above, it can be seen that as the air speed increases, the thermal time constant decreases. Furthermore, the result carries a similar one to that of the maximum temperature curves discussed earlier in this chapter. The thermal time constant does not significantly decrease when the air speed is > 3 m/s. The curves generally flatten out, as they did in the maximum temperature curve. Looking at the values in the table for a desired speed of 3-4 m/s, the time constant is reached between 4/1/2-5/1/2 minutes. It is now known how the device exponentially increases in temperature relative to time.

Finally, it can be seen that the convection coefficient and thermal time constant have a rough linear relationship, as shown in Figure 3.18 below:

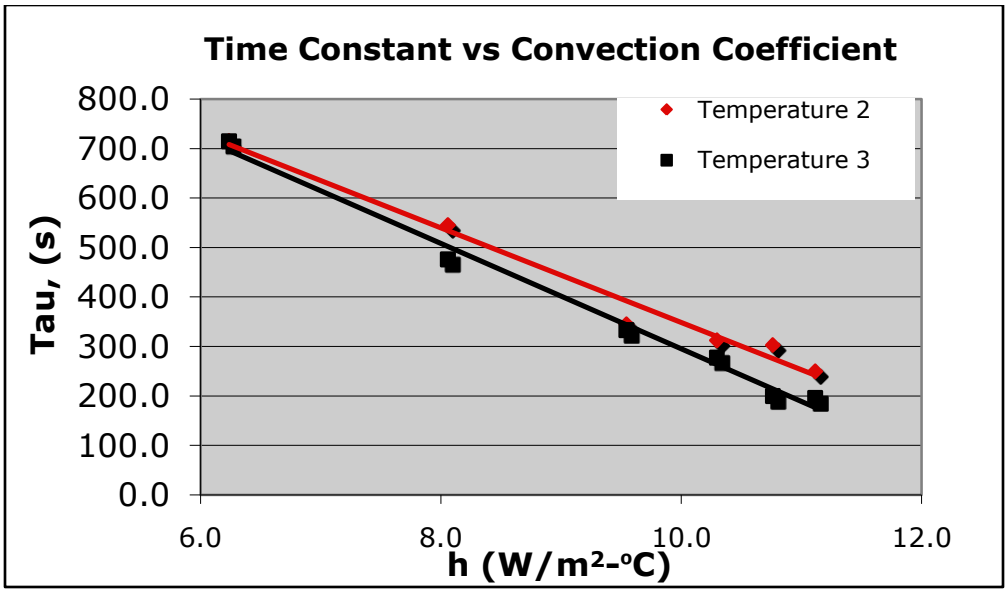

Figure 3.18: Relationship of Thermal Time Constant Against Convection Coefficient

From this, as the fan speed is increased and the convection coefficient increases, the thermal time constant decreases. Analyzing this, for this particular heat sink under such a forced convection scenario, a relationship between h and is τ known, where τ/h does not equal a constant.

3.6 Nusselt Number Correlations

3.6.1 General Equations

The goal of this forced-convection experiment is to develop experimental Nusselt number equations of the form [2];

$$Nu = C_1 Re^m Pr^n \tag{3.11}$$

where the standard Prandtl number exponent for air is assumed (n =1/3). It can be seen from Equation (3.11) that a Nusselt number correlation is directly dependent on the Prandtl and Reynolds numbers. The Prandtl number can be calculated using the temperature relation shown in Equation (3.7), where the temperature used to calculate this value is the film temperature.

The Reynolds number is a function of characteristic length. Possible length scale choices include the heat sink length (like a flat plate), and a hydraulic diameter (like co-annual tubes).

For the first case treating the heat sink as a flat plate where the characteristic length is L_c, Reynolds Number is calculated using the equation [2]:

$$Re = \frac{\overleftarrow{V_{fin}} L_C}{\nu} \tag{3.12}$$

Where L_c is .18m, and υ can be calculated using its temperature correlation with Equation (3.5). To calculate the Reynolds number, the inlet velocity (or air speed passing by the fins) is needed.

3.6.2 Expected Upstream Velocity

The propeller anemometer was used in these tests to set fan and thus air speeds throughout this experiment. Once the flow velocity was set, a velocimeter probe was used at specific locations to measure an average air speed next to the fin. The locations of all the

velocimeter readings are shown in Figure 3.19 below. As can be viewed in Figure 3.19, the first reading was taken at the top of the heat sink. For all three measurement planes; left, middle and right; the readings were taken at one centimeter increments. An average air velocity passing the heat sink, V_{fin}, can be found as an average of all 24 readings.

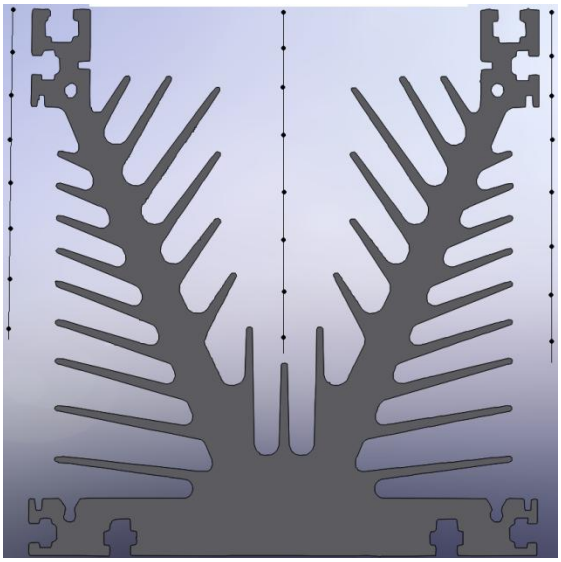

Figure 3.19: Velocimeter Locations: Left, Middle, and Right of the Heat Sink

These heat sink flow velocity measurements were verified using an alternative method which uses upstream measurements and conservation of mass. A location six inches upstream of the heat sink was chosen, and the velocimeter was used again to find forty velocity values. Their respective locations can be shown in Figure 3.20:

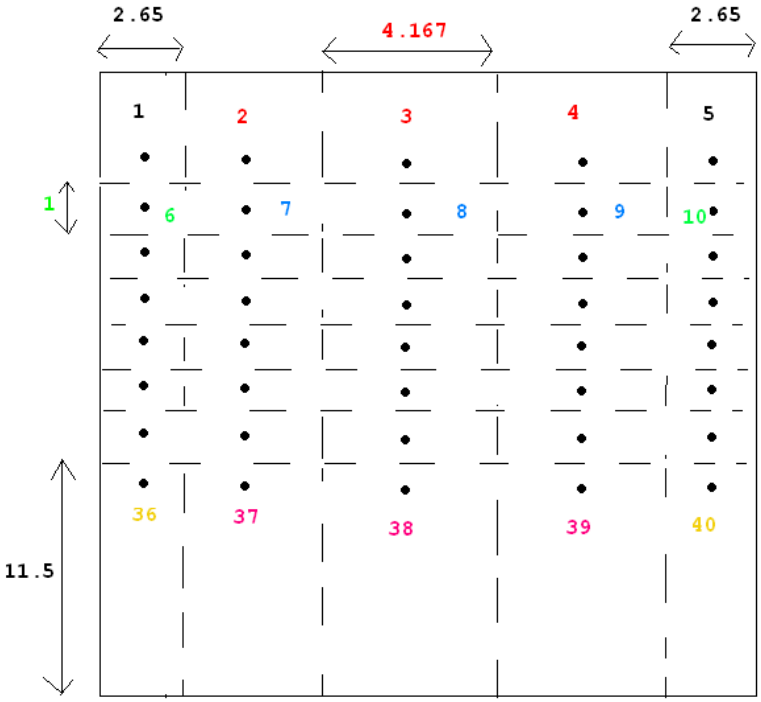

Figure 3.20: 40 Upstream Velocimeter Locations

The vertical placement of all of the readings coincides with the locations shown in Figure (3.19), i.e. velocities labeled 1-5 are vertically located at the top of the heat sink. In addition, velocities labeled 36-40 vertically coincide with the bottom readings in Figure (3.19). The same approach used to find the air velocities was also used here. These 40 readings were found for each of the six corresponding flow settings. By finding the average upstream velocity, and applying conservation of mass, an estimate of the air speed passing the fins can be found as:

$$\dot{m}_{in} = \dot{m_{out}}, \quad \rho_{upstream}\bar{\bar{V}}_{upstream}A_{upstream} = \rho_{HS}\bar{\bar{V}}_{HS}A_{HS}$$

Noting that that the density of air is nearly constant gives:

$$\bar{\bar{V}}_{upstream}A_{c,duct} = \bar{\bar{V}}_{fin,expected}A_c$$

Therefore, the air velocity passing the fins can be found in terms of the upstream average velocity as:

$$\overleftarrow{\bar{V}}_{HS,expected} = \frac{\overleftarrow{\bar{V}}_{in,avg} A_{c,duct}}{A_c} \tag{3.13}$$

Using conservation of mass with weighted area regions, the expected air velocity passing the fins can be calculated by rewriting equation (3.12) in the form:

$$\overleftarrow{\bar{V}}_{fin,expected} = \frac{\sum_{i=1}^{40} \sum_{i=1}^{40} V_{i,j} A_{i,j}}{A_c} \tag{3.14}$$

These values, along with the velocities measured next to the fin (shown in Figure 3.19) are given in Table 3.8 below:

Table 3.8: Experimental Fin Velocity Results:

V_{outlet} (m/s)	V_{fin} (m/s)	$V_{fin,expected}$ (m/s)	% Error
1	1.074	.987	8.815
2	2.356	2.294	2.723
3	3.718	3.659	1.617
4	4.978	4.952	.518
5	6.305	6.110	3.191
6	7.388	7.277	1.514

The percent error between these two measurement methods is rather small for all six flow velocities, with the slowest speed being the one outlier carrying an 8.815% error. All the other speeds give a percent error <3.191%, which is well within the range of experimental error. Velocities calculated using Equation (3.14) will be used in the Reynolds number. The outlet and heat sink air velocities, V_{fin}, were found to be linearly related, which confirms the repeatability of the experiments.

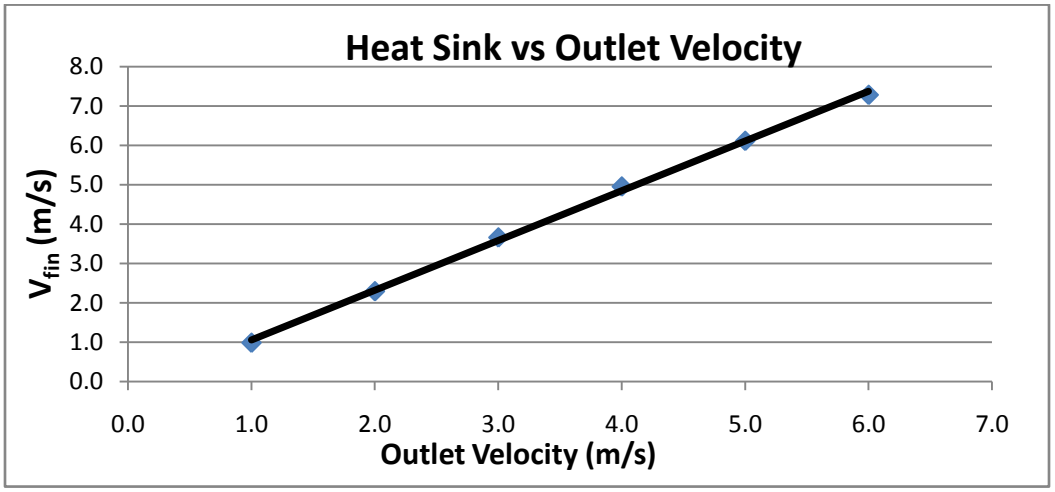

Figure 3.21: Relation of Heat Sink to Outlet Velocity

Furthermore, except for V_{outlet}=1m/s, $V_{HS}>V_{outlet}$. The air flow cross-sectional area was calculated by:

$$A_c = A_{c,duct} - (A_{c,HS} + A_{c,insulation})$$

As the value of the cross-sectional area decreases, the air velocity passing the fin increases. Because the wooden duct restricts the air flow to a confined region, the cross-sectional flow area at the location of the heat sink decreases, thus raising the value of the air velocity at the

fins. The increased values above were expected, and the duct ultimately creates a more efficient and cooler heat sink.

Now that the air velocity has been found, an important relationship between the convection coefficient, h, and the velocity can be shown. A graph of h vs. $V_{fin,expected}$ is shown below in Figure 3.22. As the velocity increases, the increasing value of the convection coefficient slows down, and ultimately reaches a peak value. Also, the range of the convection coefficient value is relatively small: $6.2\frac{W}{m^2K} \leq h \leq 11.1\frac{W}{m^2K}$. A high

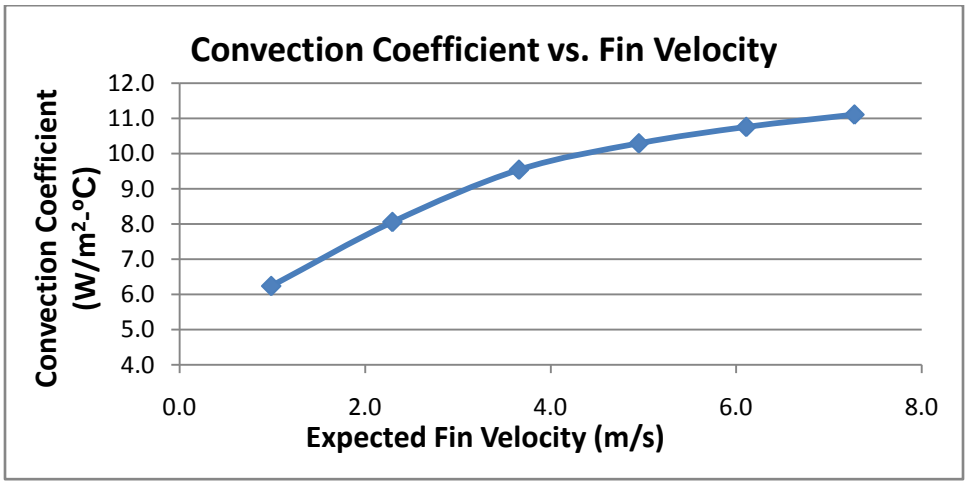

Figure 3.22: Convection Coefficient vs. Fin Velocity for One Heat Sink

convection coefficient gives a small change in temperature (ΔT) for a given heater power.

3.6.3 Remaining Heat Transfer Parameters

Now that the expected fin velocity has been found, the rest of the parameters can be calculated. All of the parameters being studied are evaluated using an average film temperature [10]:

$$T_{film}(K) = \frac{T_{max} + T_{ambient}}{2} \tag{3.15}$$

Furthermore, the value for Nusselt can also be found using:

$$Nu = \frac{hL_c}{k_{air}} \tag{3.16}$$

Using Equations (3.4)-(3.7), (3.14) where all known temperature dependencies use the film temperature calculated from Equation (3.15). Now, all experimental parameters can be found and are shown in Table 3.9 below:

Table 3.9 Values for Parameters using Film Temperature

	Eq'n (3.14)	Eq'n (3.15)		Eq'n (3.5)	Eq'n (3.4)	Eq'n (3.6)
Outlet Vel (m/s)	**$V_{fin,exp}$ (m/s)**	**T_{film} (°C)**	**T_{film} (K)**	**$\nu = \nu\ fn(T_{film})$**	**$\mu = \mu\ fn(T_{film})$**	**$k = k\ fn\ (T_{film})$**
1.000	0.987	53.362	326.512	1.985E-05	2.022E-05	0.0275
2.000	2.294	46.544	319.694	1.916E-05	1.990E-05	0.0270
3.000	3.659	43.244	316.394	1.883E-05	1.974E-05	0.0267
4.000	4.952	41.714	314.864	1.867E-05	1.967E-05	0.0266
5.000	6.110	41.151	314.301	1.862E-05	1.964E-05	0.0266
6.000	7.277	40.041	313.191	1.851E-05	1.958E-05	0.0265

3.6.4 Least-Squares Derivation

Having the values of all these air properties at the film temperature, with the expected fin air velocities found, the empirical heat transfer correlation for the Nusselt number can be

found. To begin this process starting with Equation (3.10), a least squares analysis can be used to find the two unknown constants, C_1 and m. Rewriting (3.10) using logarithms [11]:

$$\underbrace{\log(Nu)}_{Z} = m\underbrace{log(Re)}_{x} + n\underbrace{log(\mathrm{Pr})}_{y} + \underbrace{log(\mathrm{C1})}_{C} \tag{3.17}$$

Where Equation (3.16) carries the form

$$Z=Ax + By + C \tag{3.18}$$

The purpose of using logarithms is to obtain an equation that is linear, which makes solving the unknowns substantially easier. This table shown below was generated for the six flow velocities (Recall Power = 150 watts for all cases):

Table 3.10: Values at all Six Expected Fin Speeds & Resulting Logarithm Values (Flat Plate)

Pr = Pr fn(T_{film})	**Re_L**	**Nu_L**	**log(Re)**	**log(Pr)**	**log(Nu)**
0.7107	8948.142	40.887	3.952	-0.148	1.612
0.7115	21550.019	53.768	4.333	-0.148	1.731
0.7119	34980.585	64.233	4.544	-0.148	1.808
0.7120	47731.911	69.574	4.679	-0.147	1.842
0.7121	59072.440	72.829	4.771	-0.147	1.862
0.7122	70777.817	75.433	4.850	-0.147	1.878

where Prandtl, Reynolds, and Nusselt numbers are calculated using Equations (3.7), (3.11), and (3.16). Equation (3.17) carries an error between the predicted value and the actual measured value, which can be found by [11]:

$$E = e^2 = \sum_{i=1}^{N}\left(z_i - Ax_i - By_i - C\right)^2 \tag{3.19}$$

The proper way to make E a minimum from Equation (3.19) is to state [11]:

$$\frac{\partial E}{\partial A} = \sum_{i=1}^{N} 2e_i \frac{\partial e_i}{\partial A} = \sum_{i=1}^{N} 2\left(z_i - Ax_i - By_i - C\right)(-x_i) = 0 \tag{3.20}$$

$$\frac{\partial E}{\partial B} = \sum_{i=1}^{N} 2e_i \frac{\partial e_i}{\partial B} = \sum_{i=1}^{N} 2\left(z_i - Ax_i - By_i - C\right)(-y_i) = 0 \tag{3.21}$$

$$\frac{\partial E}{\partial C} = \sum_{i=1}^{N} 2e_i \frac{\partial e_i}{\partial C} = \sum_{i=1}^{N} 2\left(z_i - Ax_i - By_i - C\right)(-1) = 0 \tag{3.22}$$

Now, from looking at (3.20)-(3.22) where there are three unknowns, it can be said [11]:

$$A\sum_{i=1}^{N} x_i^2 + B\sum_{i=1}^{N} x_i y_i + C\sum_{i=1}^{N} x_i = \sum_{i=1}^{N} x_i z_i \tag{3.23}$$

$$A\sum_{i=1}^{N} x_i y_i + B\sum_{i=1}^{N} y_i^2 + C\sum_{i=1}^{N} y_i = \sum_{i=1}^{N} y_i z_i \tag{3.24}$$

$$A\sum_{i=1}^{N} x_i + B\sum_{i=1}^{N} y_i + C\sum_{i=1}^{N} 1 = \sum_{i=1}^{N} z_i \tag{3.25}$$

The easiest way to solve these equations is to use a matrix. This is the preferred method because a program such as MatLab can generate the unknown constants quickly. The resulting matrix will carry the form [11]:

$$\begin{bmatrix} \sum x_i^2 & x_i y_i & \sum x_i \\ \sum x_i y_i & \sum y_i^2 & \sum y_i \\ \sum x_i & \sum y_i & N \end{bmatrix} * \begin{bmatrix} A \\ 1/3 \\ C \end{bmatrix} = \begin{bmatrix} \sum x_i z_i \\ \sum y_i z_i \\ \sum z_i \end{bmatrix} \tag{3.26}$$

Where this matrix can be written in general form as:

$$AX=B \tag{3.27}$$

$$X=A^{-1}B$$

As I had mentioned earlier, the Prandtl number exponent for air is considered to be a constant around 1/3. Therefore, Equation (3.11) can be rewritten as:

$$Nu = C_1 Re^m Pr^{\frac{1}{3}} \tag{3.28a}$$

$$\frac{Nu}{Pr^{1/3}} = C_1 Re^m \tag{3.28b}$$

Taking a look at (3.28b), it can be seen now that there are only 2 unknowns to be found by solving this matrix instead of 3. Because the Prandtl exponent is a known quantity, the middle row and column of the matrix can be deleted, where our final matrix takes the form of a 2x2 matrix:

$$\begin{bmatrix} \sum_{i=1}^{N}(\log\ Re)^2 & \sum_{i=1}^{N}(logRe) \\ \sum_{i=1}^{N}(logRe) & N \end{bmatrix} * \begin{bmatrix} A \\ C \end{bmatrix} = \begin{bmatrix} \sum_{i=1}^{N}\left(logRe * \log\frac{Nu}{Pr^{1/3}}\right) \\ \sum_{i=1}^{N}\left|log\left(\frac{Nu}{Pr^{1/3}}\right)\right| \end{bmatrix} \tag{3.29}$$

Where:

- m=A
- n=B=1/3 (known)
- $C_1=10^C$

This is an extremely efficient method of finding an empirical heat transfer correlation for Nusselt number from experimental data. MatLab® is able to solve the 2x2 matrix. Therefore, for the first test scenario where Reynolds number is calculated considering external flow, where L_c is the characteristic length, the experimental Nusselt number is:

$$Nu = 3.086Re^{.29}Pr^{1/3} \tag{3.30}$$

As previously mentioned, the second study was considering Reynolds number for internal flow. The process for finding the Nusselt correlation is exactly the same. Starting with Table (3.9) and Equation (3.15), follow the same steps to set up the matrix, and use Matlab to generate your unknown values. Now, Reynolds number is found using a new equation holding the form [2]:

$$Re_d = \frac{\overleftarrow{V_{fin}} d_h}{\nu} \tag{3.31}$$

The Nusselt number also holds a new form with the hydraulic diameter which is:

$$Nu_d = \frac{hd_h}{k_{air}} \tag{3.32}$$

Using Equation's (3.31) and (3.32) and following the same procedure, the second empirical Nusselt number correlation found experimentally is:

$$Nu_d = .8970Re_d^{.30}Pr^{1/3} \tag{3.33}$$

It is clear from (3.33) and (3.30) that the flat plate and internal flow assumption produces two different results, where the difference lies in the constant, C_1. This happens because the value for Reynolds number drastically differs depending on which characteristic length is used. For example, Table 3.9 shows that Reynolds number ranges between 8,900 and 71,000

when L_c is the characteristic length. For a flat plate the critical Reynolds number is $5x10^5$. Therefore, for this case the flow is always in the laminar regime. By comparison, the internal flow assumption has Reynolds number value's ranging from 1,650 to 13,100, when hydraulic diameter (d_h) is the characteristic length. When using the hydraulic diameter, the critical Reynolds number is 2,300. Therefore, it appears that the flow regime has a portion in the laminar and transitional region.

The availability of convective heat transfer correlations for this heat sink can help thermal management designers. Using the Nusselt number correlations found in Equations (3.31) and (3.34), you can work backwards to solve for the convection coefficient in Equations (3.16) and (3.31) respectively. Figure 3.23 below shows that for each of the two correlations, flat plate and internal flow, fit the data well.

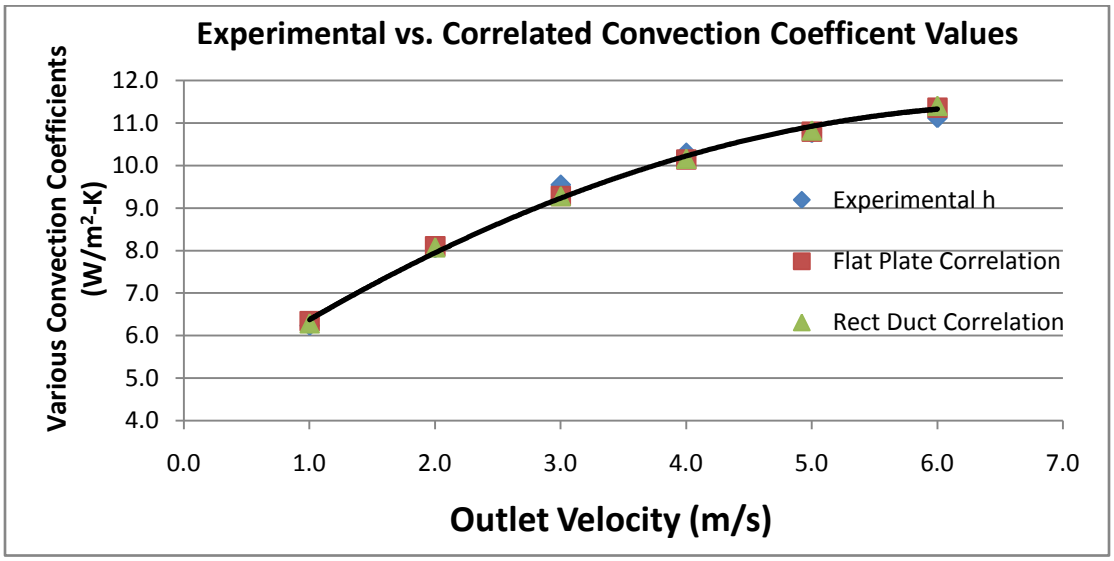

Figure 3.23: Correlated vs. Experimental Convection Coefficient Values

For all of the data, the maximum error for either case is <3%. Even though both assumptions can predict the behavior, the internal flow assumption correlation using the hydraulic diameter makes more sense for the study at hand. This assumption takes into account that the heat sink is inside a duct, whereas the flat plate assumption does not. Furthermore, the flat plate assumption is assuming that each individual heat sink fin is being analyzed as an individual flat plate, which may not be realistic. The Wakefield heat sink geometry is much more complex than that.

In addition, the exponent of the Reynolds number value can be compared to our existing correlations. For either assumption, the experimental exponent value was found to be about .3. For a quick comparison, some common Nusselt number correlations are:

- $Nu_{laminar} = .664Re_L^{1/2}Pr^{1/3}$ (flat plate, average h assumption)
- $Nu_{turbulent}=.023Re_d^{4/5}Pr^n$ (internal, fully developed flow assumption)

It can be seen that the equations shown above do have different values for the Reynolds number exponent. This may be because the flow is in a transitional flow regime. In addition, the heat sink has a complex geometry that may contribute to this difference.

3.7 Forced Convection, 2 Heat Sink Test

3.7.1 Experimental Setup

The second half of this heat sink study involves putting 2 heat sinks inside the wind tunnel. The wind tunnel shown in Figure (3.12) was used again. A picture below shows the orientation of the two heat sinks:

Figure 3.24: (a) Perpendicular View of Wind Tunnel, (b) View of Entire Wind Tunnel

Unlike the first test with only one heat sink, this test used 10 thermocouples placed at specific locations which are illustrated by the sketch below:

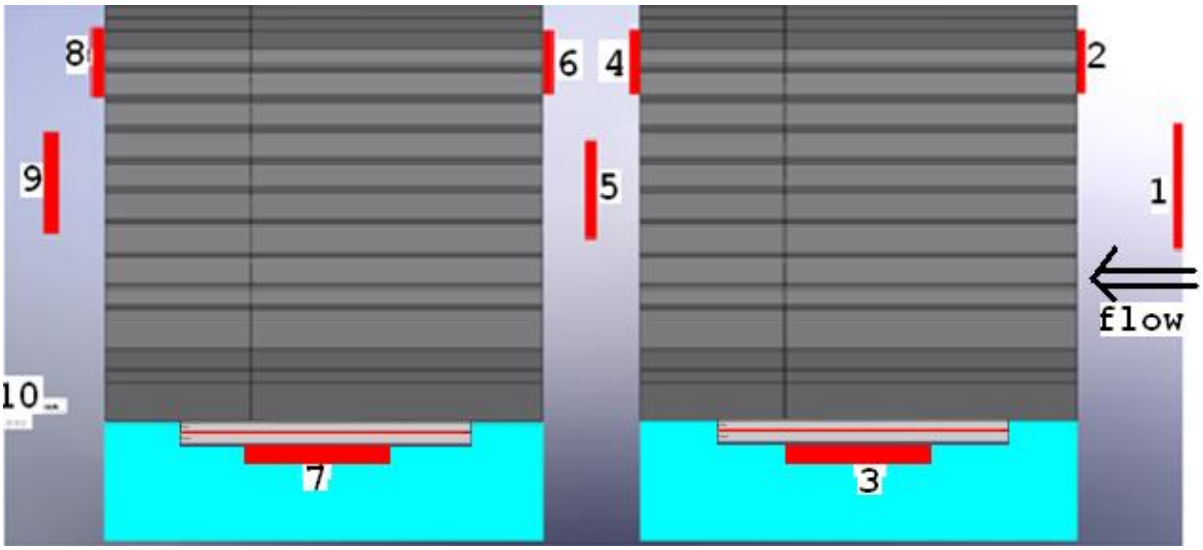

Figure 3.25: Placement for All 10 Thermocouple's for the 2 Heat Sink Test

There are some points of emphasis regarding the more relevant thermocouples. For heat sink one, the maximum temperature is measured by thermocouple 3 ($T_{max} = T_3$), and its ambient air temperature is measured by thermocouple 1. Therefore, the change in overall temperature for the first heat sink is calculated using: $\Delta T_{HS1} = T_3 - T_1$. Similarly, the overall change in temperature for heat sink two will be calculated by: $\Delta T_{HS2} = T_7 - T_5$. The main point to notice here is that the free stream temperature for heat sink two is not measured by thermocouple #1, but is measured by thermocouple #5. This distinction must be made in order to obtain the correct results.

Similar to the forced-convection test for one heat sink, this experiment was run at 1,2,3,…6m/s, where both heat sinks were heated with 150 watts. But for this test, another geometric parameter must be taken into account; the gap spacing between Heat Sink 1 and Heat Sink 2. Gap increments were also chosen as: 0,1,2,3,4, and 7 inches (the length of one heat sink is roughly 7 inches). Each spacing had to be tested at all six air speeds. The goal now is to find an efficient two heat sink system in regards to 2 parameters: Air speed, and also geometric orientation between the two devices.

3.7.2 Expected Results

By considering the geometric orientation of the device, a few observations can be made. Looking at Figure (3.20), it is evident that any heated air that is generated from the first heat sink will have to pass by the second heat sink. Therefore, the ambient air temperature that the second heat sink is receiving will be hotter than the upstream air temperature; meaning $T_5 > T_1$ for every case. Just to give a few numbers, for a 2 inch gap

spacing at 2m/s, T_1 =25.132°C and T_5 =40.103°C. What this means is that the second heat sink is receiving free flowing air which is 15°C hotter than the upstream heat sink is receiving. The maximum temperature for heat sink 2 will always be hotter than heat sink 1 (assuming they are equally powered).

3.7.3 Tabulated Results

Since all the tests were run in the same way, the 2 inch gap spacing case has been chosen for the discussion. Table 3.11 below gives the results from the DAQ device:

Table 3.11: 2 Heat Sink Forced-Convection Results for a 2 inch Gap Spacing

Outlet Vel (m/s)	Max Temp	ΔT_{max}	$T_{max,HS1}$	$\Delta T_{max,1}$	$T_{max,HS2}$	$\Delta T_{max,2}$	$\Delta T_{max,2}$- $\Delta T_{max,1}$
1	103.488	77.109	86.165	59.786	103.488	63.076	3.290
2	70.508	45.375	63.731	38.599	70.508	41.408	2.809
3	63.039	37.679	58.025	32.666	63.039	34.780	2.114
4	59.623	34.346	55.571	30.295	59.623	32.358	2.063
5	56.468	31.297	53.104	27.933	56.468	29.766	1.833
6	54.977	29.887	52.177	27.087	54.977	28.521	1.434

There are three relevant things to mention from Table 3.11. As expected, the maximum temperature of the entire system decreases as the fan speed increases. Secondly, it can be seen that the maximum temperature of the second heat sink is greater than the first for every test. Finally, the last column shows that $\Delta T_{max,2} > \Delta T_{max,1}$ for every test.

Table 3.12 summarizes the thermal resistances and convection coefficients for the tandem heat sink cases:

Table 3.12: Calculated Resistance and Heat Transfer Coefficient values

Outlet Vel (m/s)	$R_{th,HS1}$ (ºC/W)	$R_{th,HS1}$'' (ºC/W)	$R_{th,HS2}$ (ºC/W)	ΔR_{th} (ºC/W)	Perc Diff (%)	h_{HS1} (W/m^2-ºC)	h_{HS2} (W/m^2-ºC)
1	0.390	0.370	0.483	0.113	23.452	6.162	4.972
2	0.252	0.232	0.298	0.066	22.215	9.526	8.048
3	0.216	0.196	0.252	0.055	21.962	11.102	9.547
4	0.199	0.179	0.227	0.047	20.895	12.043	10.589
5	0.185	0.165	0.209	0.044	20.998	12.972	11.489
6	0.178	0.158	0.198	0.040	20.150	13.518	12.163

Recalling Table 3.2, there was a calibration constant that had to be taken into account for the first heat sink. Hence, the second column labeled "Resistance"$_{HS1}$" takes into account the .02K/Watt difference found earlier in the calibration test. From this table, it can be seen that the resistance of the second heat sink is indeed higher than the first for every single test, thus creating a performance decrease of over 20% for the second heat sink. Furthermore, this holds true at all gap spacings. The resistances and convection coefficients were calculated in the same way as earlier, using Equations (3.3) and (3.9).

3.7.4 Graphical Results

Since it is understood that for every test $T_{max,HS2} > T_{max,HS1}$, and $R_{max,HS2} > R_{max,HS1}$, only curves from the second heat sink will be shown. The form and shape of the graphs generated from the first heat sink carry the same shape, where the axis are only scaled to different values. Below are figures of the maximum temperature and difference in thermal resistances:

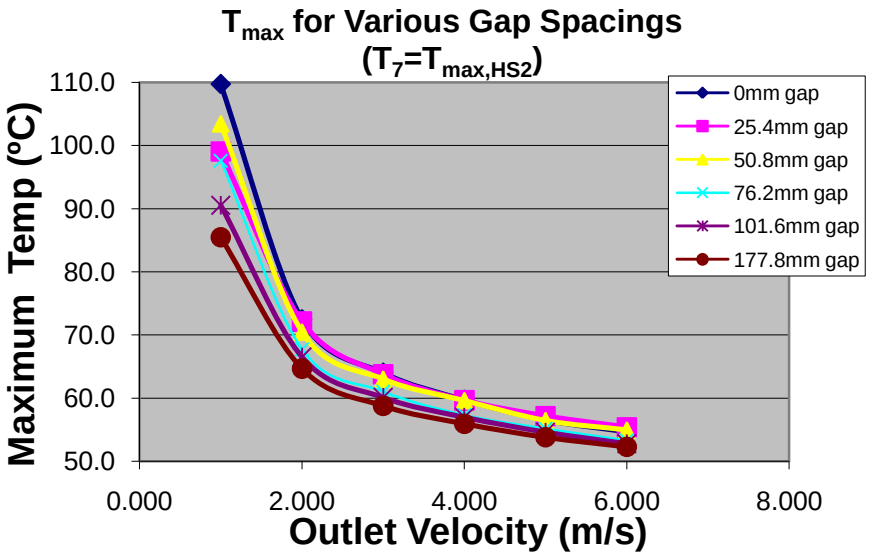

Figure 3.26: Maximum Temp for Heat Sink #2 for Various Gap Spacing's

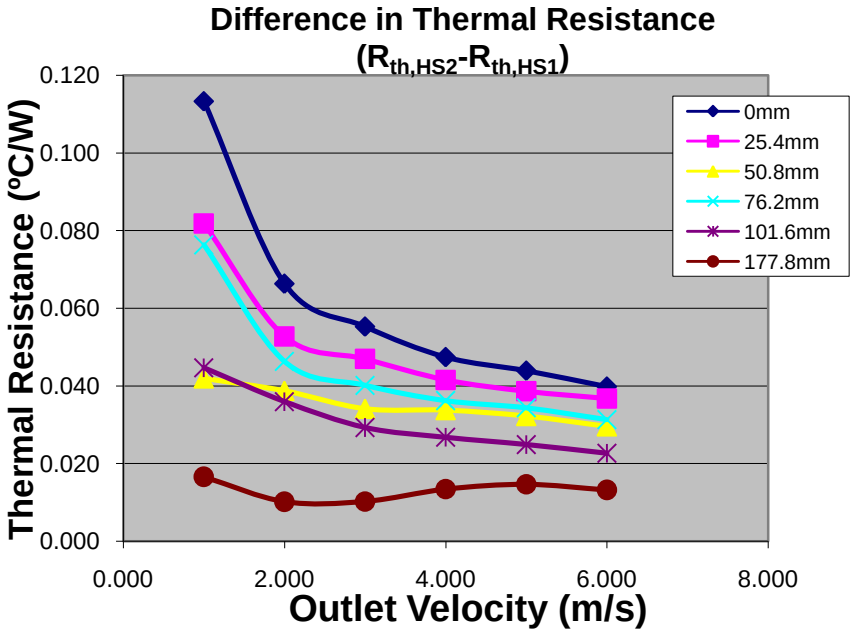

Figure 3.27: ($R_{max,HS2}$-$R_{max,HS1}$) for Various Gap Spacing's

Looking at the maximum temperature graph, a few points can be made. The maximum temperature for the one heat sink forced-convection test was 82.25°C, whereas for two heat sink forced-convection the hottest temperature produced was nearly 110°C. Therefore, there is a definite loss in performance when adding a second heat sink to the system. Similar to the single heat sink case when the system reaches 3m/s, there is only a slight gain in performance. Therefore, it is a logical choice to choose such a speed for the same reasons mentioned earlier. Finally, increased gap spacing creates only a marginal reduction of the maximum temperature. As many designs have space restrictions, it is recommended that a 1 or 2 inch gap between the heat sinks be used.

Looking at the difference in thermal resistance graph (Figure 3.27), it can be seen that as fan speed increases, the performance of the two heat sinks becomes closer (i.e. and $R_{max,HS2} \sim R_{max,HS1}$). Likewise, as the gap spacing gets larger, the difference in thermal resistances of the two heat sinks creeps closer in value. Viewing the curve for the 177.8mm gap (a 7inch gap is a full length of a heat sink), the difference in their resistances is minimal. Therefore, when a second heat sink is placed one heat sink length or more downstream of the first, the system can be interpreted as two individual heat sinks. Table 3.12 shows that there is an large difference in performance of the second heat sink relative to the first when the gap is small, whereas when a large gap is placed between them, the behavior of the two heat sinks is similar.

Table 3.13: Performance Difference for a 0 & 7 inch gap

0 inch Gap	7 inch Gap
Performance Diff (%)	Performance Diff (%)
23.452	4.483
22.215	4.226
21.962	4.940
20.895	6.924
20.998	8.060
20.150	7.585

For every arrangement, the heat transfer for the downstream heat sink is poorer in comparison to the upstream heat sink. This occurs because of the upstream heat sink is receiving unobstructed air, with no object in the way to impede its flow. The airflow impeding on the downstream heat sink is being obstructed by the upstream heat sink. As a result, the second heat sink is in the wake of the upstream heat sink. For our case, such a process produces disrupted air flow onto the downstream heat sink, thus causing it to be more thermally inefficient.

Some conclusions can be made from these results. If size and space limitations of a device were not an issue, choosing a large gap spacing would increase the overall performance of the entire system. On the other hand, the largest thermal resistance for these tests was .483K/Watt at a 0 inch gap spacing at 1 m/s. Even if the desired geometric orientation is a 0 inch gap at 3m/s air speed, the maximum temperature is 63.993°C, which may be acceptable. Figure 3.28 shows that countless variations for the two parameters (air speed and gap spacing), can be chosen depending on space restrictions, cost, desired thermal efficiency, noise level, etc…

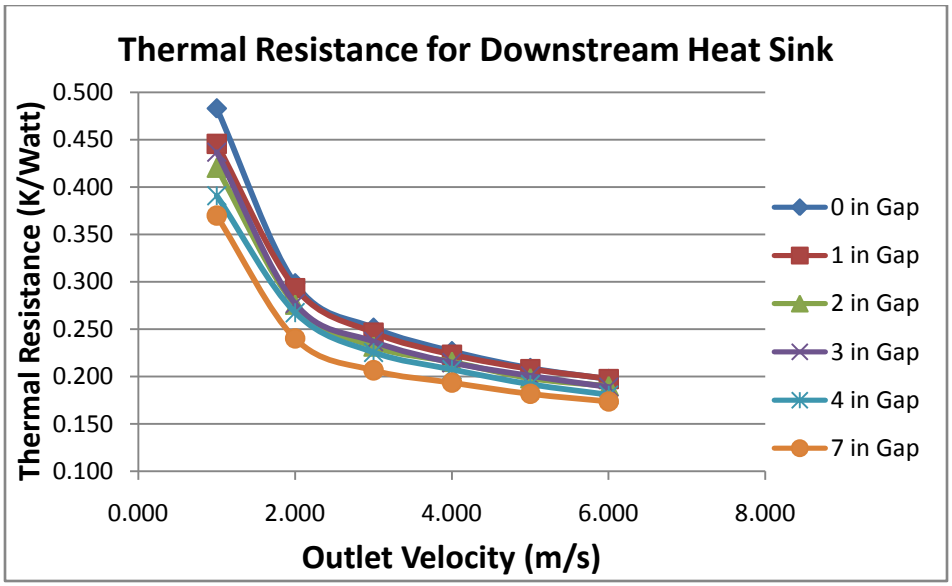

Figure 3.28: Maximum Thermal Resistance for Downstream Heat Sink

3.7.5 Nusselt Number Correlations

Now that the results for the two heat sink forced convection tests have been thoroughly discussed, the corresponding Nusselt number correlations for the devices are found next. Remembering the geometric layout of Figure 3.22, the correlations for the first heat sink will be unchanged regardless of whether the second heat sink is present. Its placement is upstream of the second device; therefore the air pattern and speed is the same as if it were by itself. Understanding this, the Nusselt number correlation for heat sink one is given by Equations (3.30) or (3.33).

Viewing Thermal Management of Microelectronic Equipment, by Yeh and Chu, where they present a correlation for equal-height modules within a fully developed flow

gives some insight to the type of correlation that may work for the second heat sink [12]. Furthermore, the gap spacing must be included in this correlation.

The same process of least-squares can be used to again solve for the unknown values in our proposed correlation given by Equations (3.34a) and (3.34b):

$$Nu_d = \frac{hd_h}{k_{air}} = C_1 Re^m \left(\frac{gap + .1}{L_c}\right)^n Pr^{1/3} \tag{3.34a}$$

$$log\left(\frac{Nu}{Pr^{1/3}}\right) = mlog(Re) + nlog\left(\frac{gap + .1}{L_c}\right) + \log(C_1) \tag{3.34b}$$

Performing a least squares fit to our experimental data gives the second heat sink as:

$$Nu_d = .4Re_d^{.406}\left(\frac{gap + .1}{L_c}\right)^{.182} Pr^{1/3} \tag{3.35}$$

- where L_c is length of the heat sink [meters].
- Where the "gap" is the space between the two heat sinks [meters].

3.7.6 Analyzing & Interpreting the Results

It is important to verify how well this correlation predicts the behavior of the second heat sink. Equation (3.35) can now be solved for all 36 cases to obtain h where the experimental and correlated convection coefficient values can be compared. Because the desire is to have a minimal gap between the heat sinks, the results for a one inch gap and two inch gap are shown in Figures 3.29 and 3.30 below:

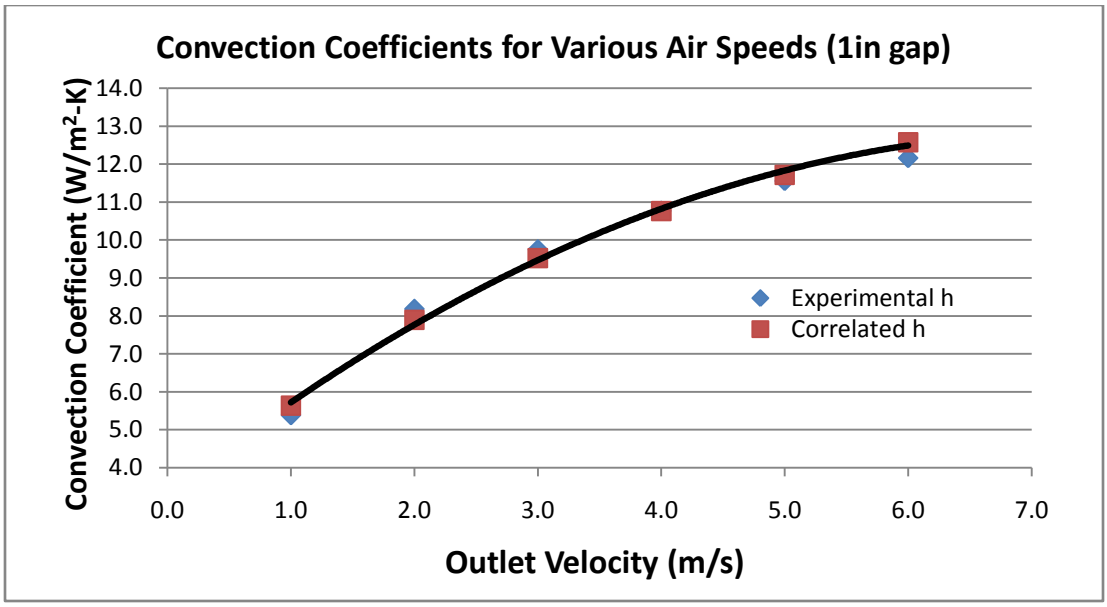

Figure 3.29: Comparison of HS_2 Convection Coefficient Values for a 1 inch Gap Space

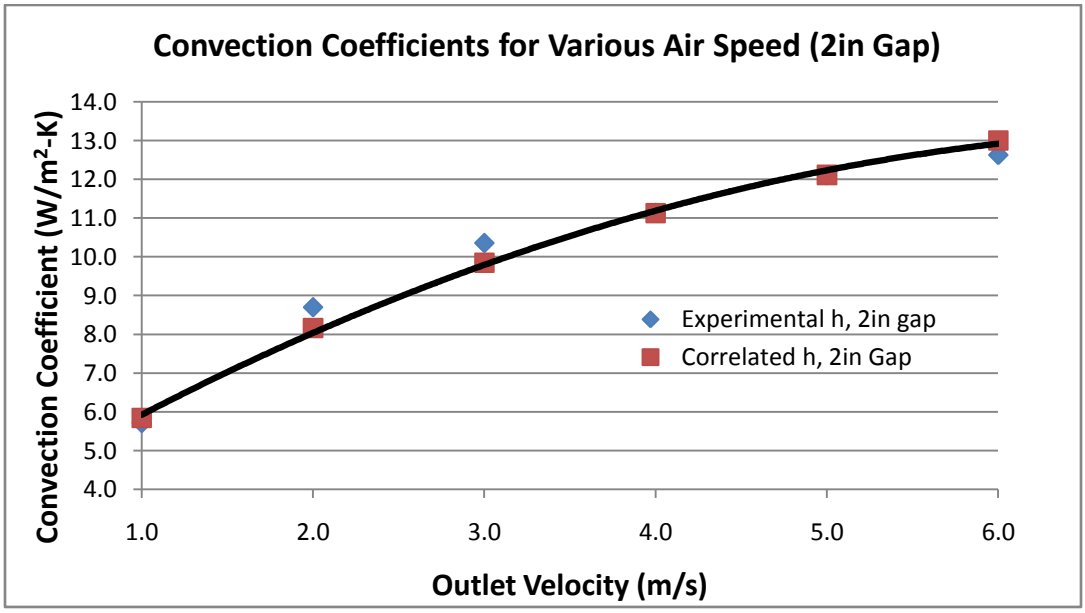

Figure 3.30: Comparison of HS_2 Convection Coefficient Values for a 2 inch Gap Space

Viewing the two figures above, it can be stated that the Nusselt correlation in (3.35) can predict the behavior of the second heat sink extremely well. For either of the two graphs, the largest error is roughly < 5%. For all of the gap spacings, the percent error is extremely small.

In addition, it can briefly be mentioned that the Reynolds number for the second heat sink is quite similar to that of the first heat sink. Recall the equation for Reynolds number shown in Equation 3.31 where the hydraulic diameter is the characteristic length, the hydraulic diameter is a constant. In addition, conservation of mass requires that the velocity at the fins is also the same. Therefore, the value in the Reynolds number will differ only by the minor change in values in kinematic viscosity, ν; which is dependent on the film temperature. This value in temperature differs between the two heat sinks. Finally, the range of Reynolds numbers for the downstream heat sink is $1495 \leq Re_d \leq 13150$. If we remember from the previous section, it was concluded that the internal flow assumption has a critical Reynolds Number of 2300. Therefore, the second heat sink also lies in the laminar and transitional regime. Finally, it should be mentioned by viewing Equations (3.30) and (3.33), that (3.35) differs only by the extra term which takes into account the gap spacing present.

Furthermore, it can be briefly mentioned that the Biot numbers for the second heat sink in the tandem study are extremely similar to the values aforementioned in the one heat sink test. Values for the Biot number range from $.4 < Bi\# < 1.35$, which are all greater than .1. Similar to the single heat sink test, these ranges of values state the temperature gradient in the system is important. In addition, there will again be a large temperature difference between the base temperature and tip temperature. A sample of DAQ steady-state temperature results

is shown again for a 1inch gap space at 3 m/s to validate these statements, where each reading was taken in 10 second increments.

Table 3.14: Sample Data, DAQ Steady-State Results for 1inch Gap

Test 3:	**3m/s**								
Sensor 1 (ºC)	**Sensor 2(ºC)**	**Sensor 3(ºC)**	**Sensor 4(ºC)**	**Sensor 5(ºC)**	**Sensor 6(ºC)**	**Sensor 7(ºC)**	**Sensor 8(ºC)**	**Sensor 9(ºC)**	**Sensor 10(ºC)**
24.486	31.978	74.365	33.392	27.015	39.202	70.976	39.662	25.502	27.094
24.528	32.036	74.409	33.398	26.866	39.166	70.912	39.640	25.476	26.838
24.515	31.988	74.386	33.338	26.944	39.151	70.712	39.711	25.541	26.958
24.521	32.000	74.352	33.364	26.913	39.117	70.725	39.592	25.549	26.991
24.546	32.090	74.454	33.463	26.944	39.217	70.877	39.701	25.585	26.876
24.421	32.025	74.446	33.396	26.889	39.181	70.851	39.720	25.554	26.888

CHAPTER 4

Copper Heat Spreader Analysis

4.1 Design Scenario

This section of the paper will focus on the study of various geometric parameters. If this heat spreader can be optimized, it can then be mounted onto the heat sink that has been tested in the previous section of this paper. Test simulations will be run using ANSYS® for each of the geometric layouts, and thermal results can ultimately be interpreted and analyzed. By generating a thermal distribution for each test scenario, the overall constriction resistance for the device can be mathematically calculated. By determining which geometric layout will yield the lowest constriction resistance, the optimal design for the electrical device can be found. All of the defining parameters that are held constant or varied in each test will be discussed, and numerous graphs for these parameters will be produced.

Although many of the parameters will be changed throughout the study, it is important to show the standard layout of the device. It is shown below:

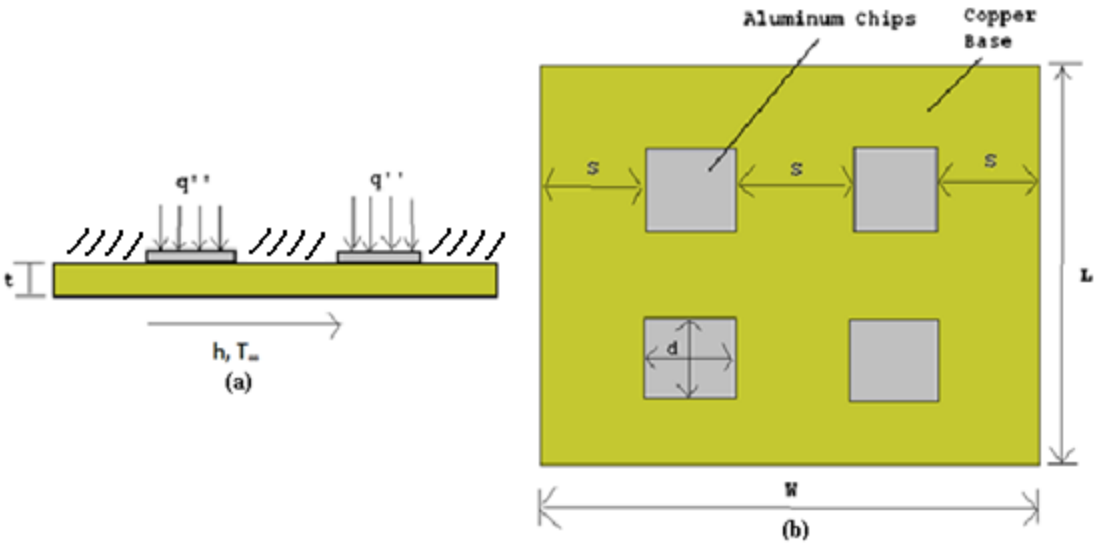

Figure 4.1: (a) Front View of Copper Heat Spreader with Location of Heat Flux and Convection Coefficient, (b) Top view & Dimensions of Heat Spreader

For all of the test scenarios, the device was always symmetric. The four aluminum chips each share equal dimensions where the length and width are both denoted by "d". All three gap spaces, "s" between each of the chips are also the same. Finally, each of the four chips will produce the same amount of power output into the device, 20 watts, therefore producing a symmetrical thermal distribution.

4.2 Various Base-Plate Thicknesses for Numerous Chip Sizes

4.2.1 Known Parameters

The first test simulation focused on the effect of changing the copper base-plate thicknesses over a range for six different aluminum chip sizes. Before this is analyzed, it is important to show a table of all the parameters that were held constant during this test. This table is given below:

Table 4.1: Constant Parameters for Test 1

Ambient Temperature (Air)	T_∞	20	^oC
Thermal conductivity (Cu)	K_{copper}	401	W/m-^oC
Thermal conductivity (Al)	K_{AL}	125	W/m- ^oC
Power Output/chip	**q**	20	W
Surface Area, Copper	$A_{s,CU}$	0.0001	m^2
Aluminum Thickness	t_{AL}	0.003	m
Convection Coefficient	**h**	20	W/ m^2- ^oC
Width, Length (Cu)	$W_{CU}=L_{CU}$	0.1	m

As seen in Figure (4.1a) above, the free stream convection coefficient and the ambient air temperature are prescribed at the bottom face of the copper, which is set to a standard free stream value of 20 W/ m^2- ^{o}C, and a standard room temperature of 20^{o}C. Both the thermal conductivity of the aluminum and the copper are held constant throughout the numerous simulations. Furthermore, as mentioned in the previous paragraph, each of the four aluminum devices has a set power output of 20 watts, which will be a constant value held through all of the studies discussed in this experiment. It can also be seen that the surface area of the copper plate does not change, where the length and width of the plate are held at a value of 100mm each.

4.2.2 Tabulated Results

To test the effect of any parameter to create an optimal design, it is important to make all other parameters constant. By doing this, the results produced will directly relate to the

overall effect of that particular parameter. For test one, four different design scenarios were tested: 2.5mm, 5mm, 7.5mm, and 10mm copper base plate thickness:

Table 4.2: Varying Parameters for Copper Base Plate = 2.5mm

W = L (mm)	d (mm)	s (mm)	q'' (W/m^2)	s/d	t/d	ΔT (°C)	T_{max}(°C)	R_{th} (W/m^2-°C)
100	10	26.67	200000.00	2.67	0.25	12.86	430.10	0.161
100	15	23.33	88888.89	1.56	0.17	8.31	425.78	0.104
100	20	20.00	50000.00	1.00	0.13	6.06	423.80	0.076
100	25	16.67	32000.00	0.67	0.10	4.57	422.61	0.057
100	30	13.33	22222.22	0.44	0.08	3.44	421.81	0.043
100	35	10.00	16326.53	0.29	0.07	2.51	421.24	0.031

Table 4.3: Varying Parameters for Copper Base Plate = 5mm

W = L (mm)	d (mm)	s (mm)	q'' (W/m^2)	s/d	t/d	ΔT (°C)	T_{max}(°C)	R_{th} (W/m^2-°C)
100	10	26.67	200000.00	2.67	0.50	9.12	427.75	0.114
100	15	23.33	88888.89	1.56	0.33	5.43	424.17	0.068
100	20	20.00	50000.00	1.00	0.25	3.94	422.80	0.049
100	25	16.67	32000.00	0.67	0.20	2.91	421.92	0.036
100	30	13.33	22222.22	0.44	0.17	2.19	421.36	0.027
100	35	10.00	16326.53	0.29	0.14	1.80	421.02	0.022

Table 4.4: Varying Parameters for Copper Base Plate = 7.5mm

W = L (mm)	d (mm)	s (mm)	q'' (W/m^2)	s/d	t/d	ΔT (°C)	T_{max}(°C)	R_{th} (W/m^2-°C)
100	10	26.67	200000.00	2.67	0.75	8.65	427.75	0.108
100	15	23.33	88888.89	1.56	0.50	4.85	424.02	0.061
100	20	20.00	50000.00	1.00	0.38	3.27	422.52	0.041
100	25	16.67	32000.00	0.67	0.30	2.38	421.73	0.030
100	30	13.33	22222.22	0.44	0.25	1.79	421.24	0.022
100	35	10.00	16326.53	0.29	0.21	1.34	420.91	0.017

Table 4.5: Varying Parameters for Copper Base Plate = 10mm

W = L (mm)	d (mm)	s (mm)	q'' (W/m^2)	s/d	t/d	ΔT (°C)	T_{max}(°C)	R_{th} (W/m^2-°C)
100	10	26.67	200000.00	2.67	1.00	8.24	427.58	0.103
100	15	23.33	88888.89	1.56	0.67	4.51	423.90	0.056
100	20	20.00	50000.00	1.00	0.50	2.98	422.43	0.037
100	25	16.67	32000.00	0.67	0.40	2.15	421.67	0.027
100	30	13.33	22222.22	0.44	0.33	1.61	421.21	0.020
100	35	10.00	16326.53	0.29	0.29	1.21	420.90	0.015

It can be seen from the tables above, that for each of the four design scenarios, six simulations were run for a chip size ranging from $10mm \leq d \leq 35mm$, and the size of the copper plate is being held constant. Recalling Figure (4.1), the width can be found by:

- w = L = 2d+3s = 100mm

Therefore, the spacing gap can be found by the formula:

$$s = \frac{w - 2d}{3} \tag{4.1}$$

The importance from Equation (4.1) is that the copper width is held constant. Therefore, as the size of the aluminum chip (d) increases, the gap spacing (s) decreases. The main focus of the results will be on the relation between the chip spacing and chip size, which is why a column denoted as "s/d" has been generated. Finally, there is a column for the heat flux, which can easily be calculated by [2]:

$$q'' = \frac{q}{A_{C,Al}} \tag{4.2}$$

For each chip, the heat flux can be calculated by taking the constant power value of 20 watts, and dividing it by the chip surface area for which the heat flux is exposed to. This is a changing value over the range of six chip sizes.

4.2.3 ANSYS®

A steady-state thermal analysis test was run for each of the various geometries in ANSYS®. After each simulation has been run, the program automatically produces the maximum and minimum temperature values on the device. An example of one thermal distribution produced in ANSYS® is shown in Figure (4.2).

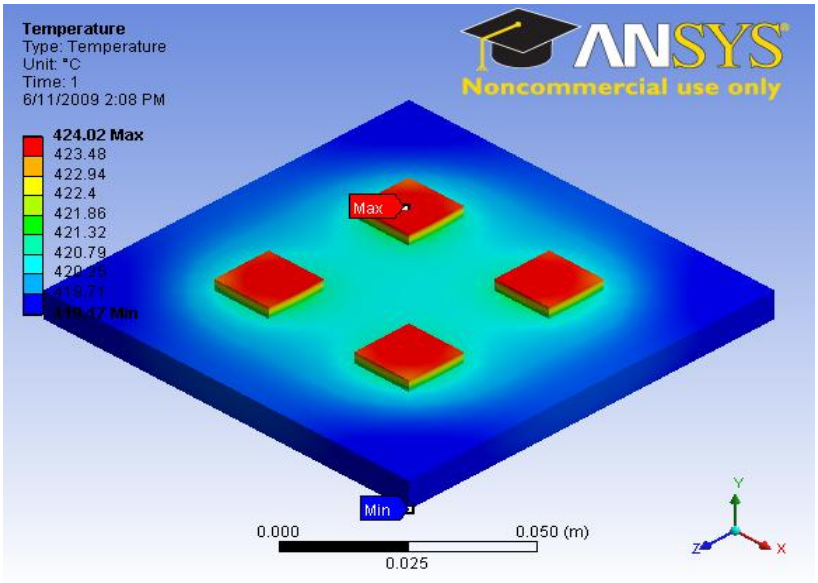

Figure 4.2: Thermal Distribution in ANSYS

Generating a thermal distribution in ANSYS® can be done in a few steps. A mesh must be created for the entire body prescribed in the program. Once a mesh has been created, the

prescribed boundary conditions must be applied to the body. In the case of this study, a constant convection coefficient of 20 W/m-^{o}C and ambient temperature of 20 ^{o}C is applied to the bottom face of the copper. Furthermore, a constant heat flux is applied to each of the four aluminum chips. This must be applied to each of the six different chip sizes for all four of the test scenarios. Once this has been done, the constriction resistance is the last parameter that must be calculated. It can easily be found by:

- $q = \frac{T_{max} - T_{min}}{Resistance}$, and substituting in Equation (4.2):
- $q'' A_{s,Al} = \frac{\Delta T}{R}$

Because the power is held constant through all the simulations, and having ANSYS® generate all temperature distributions, the resistance for each particular device can be found from the simple equation:

$$R = \frac{\Delta T}{q'' A_{C,Al}} \tag{4.3}$$

4.2.4 Graphical Results

By taking these results from ANSYS®, the relationship between the temperature and resistance parameters for each of the four copper thicknesses are plotted in Figure 4.3 against the changing geometrical values of the chip size and spacing. Thus, conclusions can be drawn on the affect of chip size, chip spacing, and thickness of a copper base plate heat spreader.

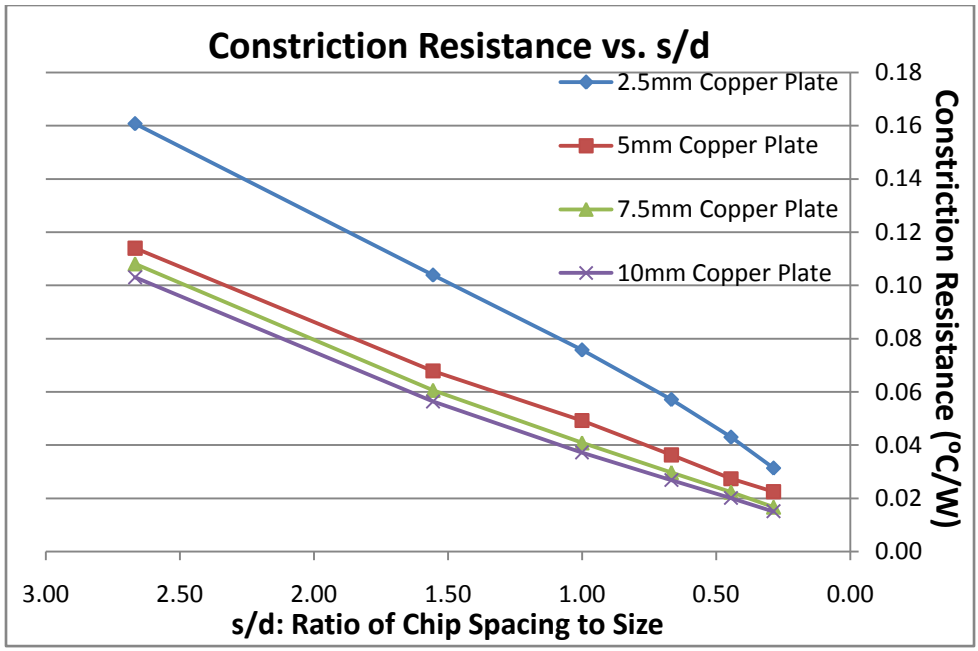

Figure 4.3: Resistance vs. chip spacing/chip size for Various Copper Thicknesses

By interpreting the x-axis as it goes from left to right, as the ratio of s/d is getting smaller, the size of the chip size gets larger. Consequently, the spacing between the aluminum chips decreases. What this graph shows is that as the size of the chip gets larger, the overall constriction resistance decreases by a factor of roughly five from the first case (d=10mm) to the last case (d=35mm). Taking a closer look at the figure above and at Tables (4.1)-(4.4), the total change in constriction resistance slows down as the chip size gets larger. What this means is there is a much larger change in the resistance from varying the chip size from 10mm to 15mm (.05 C/W), as opposed to 20mm-35mm (.02 C/W). Therefore, it may be concluded that increasing the chip size past an s/d ratio of 1:1 is most likely not worthwhile, and could possibly be a waste of aluminum material.

One more important conclusion that can be drawn is the distinction between the 2.5mm copper plate in comparison to the other three plate thicknesses. There is a clear gap in resistance values between a 2.5mm and 5mm plate, but there is minimal change for the 5mm, 7.5mm, and 10mm copper plate. Hence, choosing a 5mm copper spreader and not the 2.5mm copper spreader is wise, but choosing anything thicker might not be cost effective.

The second graph produced for this test was the relation of maximum temperature to s/d. The graph is shown below in Figure 4.4:

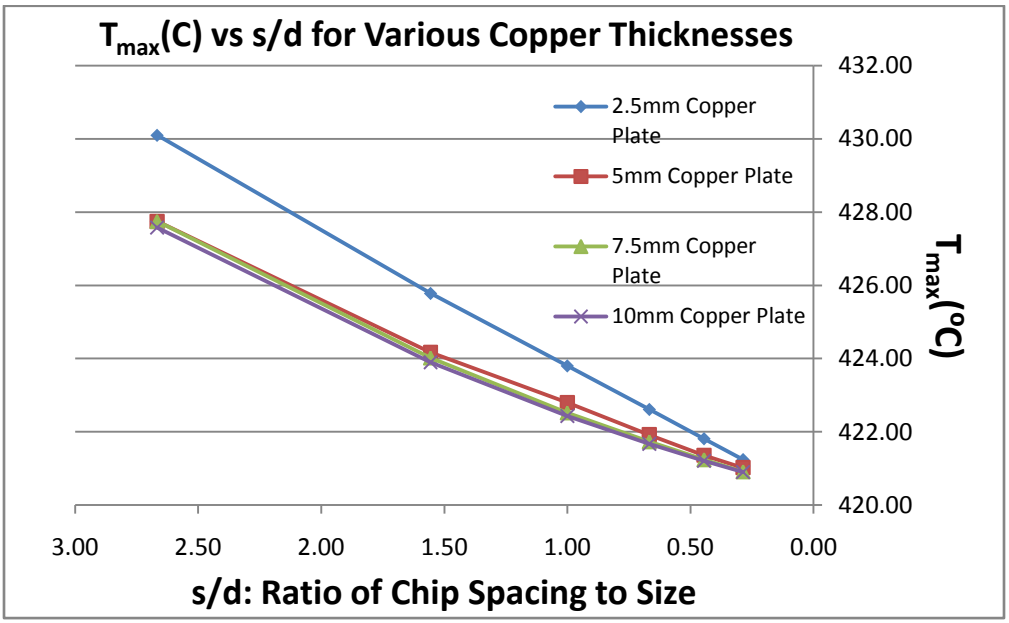

Figure 4.4: Maximum Temp vs. chip spacing/chip size for Various Copper Thicknesses

The most important aspect of this graph generated above is to show the minimal affect on the change in overall maximum temperature from increasing the thickness of the copper spreader. It can also be seen from the curves that maximum temperature does indeed

decrease as the chip size increases; yet, the range of the temperatures is roughly 10°C. Therefore, it can be said that changing the base plate thickness has almost no affect on the maximum temperature, and increasing the chip size has a minor affect.

4.2.5 Recap

To make an optimal design, every geometric parameter must be tested to see its overall affect. In this test, the two geometric parameters that were tested were the copper base plate thickness while varying the size of the power source. The graphical results allowed for some conclusions to be drawn. Firstly, as the size of the chip gets larger, the overall constriction resistance decreases. But, it is important to notice that there is only fractional affects after an s/d ratio of 1:1. Second, there is a definite gap in resistance values for the 2.5mm thick copper spreader, while the other three thicknesses have similar results. Therefore, a spreader thickness of 5mm-7.5mm will definitely want to be used. Furthermore, increasing the thickness of the copper and size of the aluminum chips only minimally decreases the maximum temperature. In the next test, it will be discussed which parameter directly affects the outcome of the maximum temperature values.

4.3 Changing Base Plate Size over Various Chip Sizes

4.3.1 Tabulated Results

This second test focused on the effect of changing copper heat spreader dimensions for various chip sizes. Test 2 will also been done to further validate the result found in the

first test. In this test there are three different design scenarios; the first contains an aluminum chip of size 10mm, the second has a chip size of 20mm, and the last being 30mm. Similar to the previous test, each scenario has six cases, where this time the copper plate has varying dimensions ranging from $65mm \leq w = l \leq 140mm$. An example of one of the three summary tables for the 10mm chip is given in Table 4.6 below:

Table 4.6: Varying Parameters for Aluminum Chip =10mm

d (mm)	s (mm)	W=L (mm)	q'' (W/m^2)	s/d	w/d	ΔT (°C)	T_{max} (°C)	R_{th} (°C/W)
10	15	65	200000	1.5	6.5	8.86	974.37	0.110
10	20	80	200000	2	8	9.21	652.9	0.115
10	25	95	200000	2.5	9.5	9.51	471.36	0.118
10	30	110	200000	3	11	9.77	358.95	0.122
10	35	125	200000	3.5	12.5	9.98	284.56	0.124
10	40	140	200000	4	14	10.23	232.82	0.127

For all of these three scenarios, the same increments for the dimensions of the copper plate were used. Each scenario starts out with the plate being 65m in length and width, and increasing to 140mm by increments of 15mm. Therefore, the spacing for each scenario within each case is found in the same way using Equation (4.1). Looking at Equation (4.2), it can be seen that because the size of the chip in each scenario is constant, the heat flux will also be constant for each of the three test scenarios.

4.3.2 Given Constants

It should briefly be mentioned that this test also has defined constant parameters, where the copper thickness is now a constant, and the dimensions are now the changing variable.

Table 4.7: Constant Parameters for Test 2

Ambient Temperature (Air)	T_∞	20^0C
Thermal Conductivity (Cu)	K_{copper}	401 W/m-ºC
Thermal Conductivity (Al)	K_{AL}	125 W/m- ºC
Power/Chip	q	20 W
Surface Area (Aluminum)	$A_{s,AL}$	.0001, .0004, .0009 m^2
Copper Thickness	t_{CU}	.005m
Aluminum Thickness	t_{AL}	.003m
Convection Coefficient	h	20 W/ m^2- ºC

The list of known parameters is shown above. Notice that all three values for the surface area of the aluminum chips have been put into the table.

4.3.3 Graphical Results

To test the effect of the changing copper plate dimensions for three different aluminum chip dimensions, ANSYS® was used to run another steady-state thermal analysis. The first graph generated, shown in Figure 4.5, is the constriction resistance plotted against the ratio of w/d. This graph has been produced to see if changing the copper plate dimensions will have any effect on the overall value of the resistance. The graph is shown below:

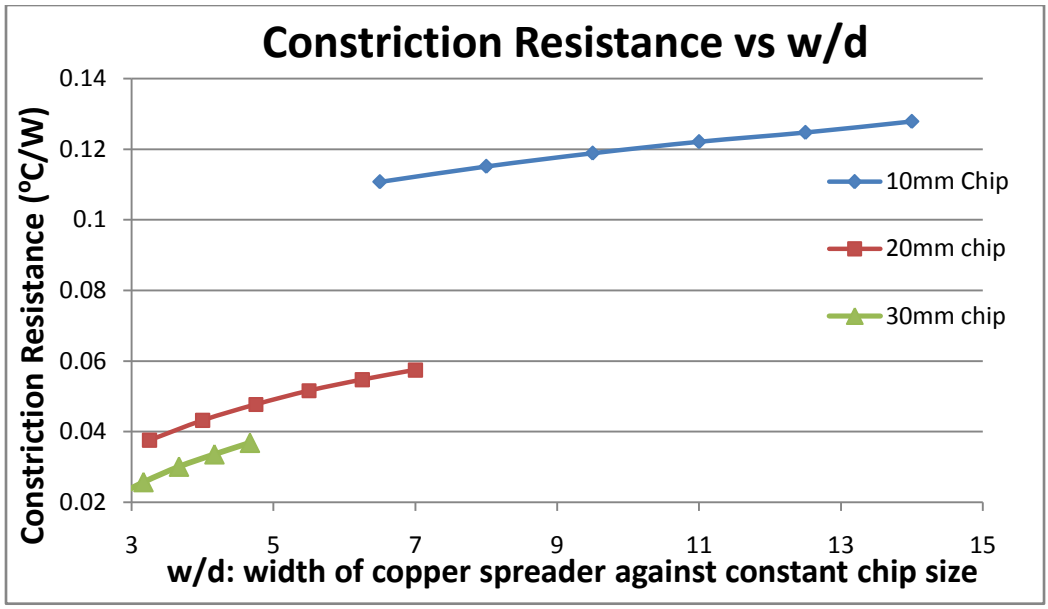

Figure 4.5: Constriction Resistance vs. Increasing Width of Copper Plate/Chip Size

On this graph it can be seen that as we travel along the x-axis, the size of the copper plate is increasing. Carefully looking at the curves generated, the results are parallel to the ones found in the previous test. Earlier it was stated that as the size of the aluminum chip increased, the overall constriction resistance value diminishes. There is a large difference in the value of constriction resistance between the 10mm chip in comparison to the 20mm and 30mm chips. There is still a decrease from the 20mm chip to the 30mm chip, but not nearly as large. This shows that the constriction resistance is extremely dependent upon the size of the aluminum chip in which the power is being produced. This graph also shows that an increase in overall size of the copper plate does not significantly increase the value of the constriction resistance, in comparison to the effect the size of the aluminum chip has. Each of the three curves has a slight change in total resistance of roughly .02 ºC/W. This result

coincides with test one showing that the constriction resistance is heavily dependent on the surface area of the aluminum chips, and only slightly dependent upon the thickness and dimensions of the copper heat spreader.

The second graph generated for this second test scenario was for the maximum temperature for each case against plotted against the ratio of w/d. The graph generated in Figure 4.4 proved that the overall maximum temperature hardly changed as the size of the aluminum chip increased. Viewing Figure 4.6 below, for each of the three chip sizes, they all carry very nearly the same maximum temperatures at each of the six cases.

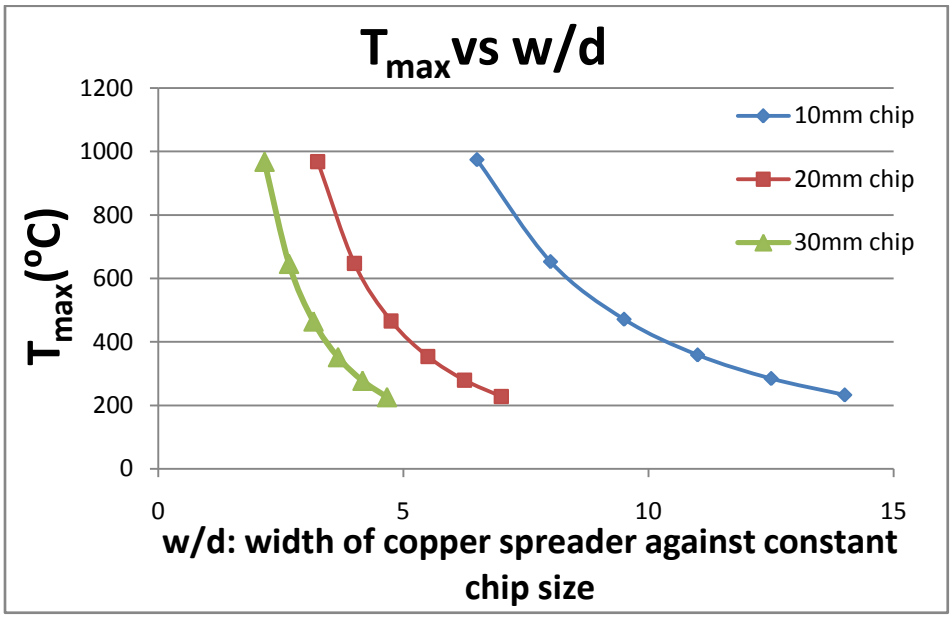

Figure 4.6: Maximum Temperature vs. Increasing Width of Copper Plate/Chip Size

For the first point, the maximum temperature for all three aluminum chips are around 990ºC, the next being around 650ºC, etc… The most important thing that can be taken from this graph is the extremely negative slope that all three of the curves carry, emphatically showing

that if the surface area of the copper heat spreader is increased, the maximum temperature drastically declines. For example, for any of the three chip sizes mounted on a 65mm spreader has a maximum temperature near 1000ºC, whereas a spreader of 140mm has a maximum temperature around 225ºC. This occurs because the bottom surface of the spreader is subjected to convection. Resistance due to convection is found by [2]:

$$R_{conv} = \frac{1}{hA_{s,Cu}} \tag{4.4}$$

Therefore, it can be seen from Equation (4.4) that the thermal resistance due to convection is entirely dependent upon the surface area of the copper plate, and the convection coefficient value. As the surface area increases, the total value of the resistance due to convection will decrease. Consequently, the results generated in Figure (4.6) coincide with Equation (4.4) shown above. Resistance due to convection will always be the determining factor in the maximum temperature the system carries. The larger the wetted surface area (and higher the convection coefficient value), the lower the maximum temperature will become.

4.4 Recap of the Results:

The device that was studied was an assembly containing four power producing chips mounted to a copper heat spreader. Thermal affects due to geometric parameters were tested in 2 different studies using the computer program ANSYS®. The first test focused on the effect of changing copper base-plate thicknesses for a range of various chip sizes. Four different spreader thicknesses were tested, including 2.5mm, 5mm, 7.5mm, and 10mm. The

second test focused on the effect of changing the copper heat spreader dimensions for various chip sizes. The three chip sizes were 10mm, 20mm, and 30mm over a range of spreader dimensions from 65mm to 140mm in length.

Figure (4.3) showed that the constriction resistance is heavily dependent upon the size of the aluminum chips in which the power is being produced. The larger the chip, the lower the resistance becomes. It also confirmed that the resistance is only slightly affected by the thickness of the copper heat spreader. There is a significant increase in the resistance value between a 5mm and 2.5mm thick copper plate. Yet, from 5mm-10mm, the resistance is nearly the same value. Therefore it is almost certainly not practical to increase the spreader thickness to anything larger than 7.5mm.

Figure (4.4) validated two facts regarding maximum temperature. Changing the thickness of the copper spreader or the surface area of the aluminum chips both have nearly no affect on the steady-state maximum temperature value. This is due to the fact that neither of these changing parameters increases the convective wetted surface area.

Figure (4.5) further validated the conclusions drawn from Figure (4.3), for which the total value of the constriction resistance is heavily dependent on the size of the aluminum chip. Furthermore, this figure also showed that drastically increasing the surface area of the copper spreader only has a slight affect on the change in value of the resistance. All three curves have a small slope, as seen in Figure (4.5), which indicates that spacing between the chips does not affect the thermal resistance values.

Finally, Figure (4.6) validates a conclusion drawn from Figure (4.4) for which the size of the aluminum chip does not affect the final value of the maximum temperature. In

addition, the maximum temperature is extremely sensitive to the size of the surface area of the copper spreader. As the spreader surface area is increased, there is an large decrease in the value of the maximum temperature.

All of the geometric parameter studies allows for conclusions to be drawn regarding an optimal design. Making the copper spreader a thickness in the range of 5mm-10mm allows for a reduction in the resistance. A larger chip surface area for which the power can be dissipated allows for a reduction in constriction resistance. Yet, the spacing between the chips, no matter what size they might be, will not be a dominating geometric parameter in this design. Finally, the larger the dimensions of the copper spreader, the lower the maximum temperature will be. Although this geometric parameter is important, the maximum temperature value can also be counteracted by an increase in a possible forced convection coefficient value. The most important things to take from these tests are:

- Increasing the power source (size of the aluminum chip) decreases the thermal resistance
- Copper spreader thickness should be in the range of 5mm-10mm
- The spacing parameter, “s” is not of great importance
- The larger the wetted surface area of the spreader, the cooler the device will be
- Increased convection values across the bottom face will drastically decrease the maximum temperature.

By maximizing the performance of a copper spreader without a heat sink being present, this geometric orientation can be added to the top of the heat sink that was optimized in Chapter 3, to generate a completely optimized design scenario.

CHAPTER 5

Concluding Thoughts

5.1 Experiments in Review

The purpose of this paper was to lay a foundation and understanding to how companies optimize their heat sink products in order to create effective cooling of electronic devices. Once this was discussed, an experiment using a Wakefield Engineering 392-High Performance Heat Sink was conducted under numerous test scenarios, in order to obtain maximum temperature and thermal resistance values. Once this was completed, a Nusselt number correlation was developed. Finally, a copper base plate heat spreader with 4 power devices was geometrically optimized. Once optimization was complete, such a device could ultimately be mounted to any heat sink.

The first portion of this paper involved reviewing a previous experiment in which a heat sink was geometrically optimized. Parameters such as fin height, thickness, frequency, and base plate thickness were analyzed. Results showed that it is ideal for a heat sink to contain long, thin fins which allow for a large wetted surface area. This creates a high perimeter to fin cross-sectional area ratio, which is ideal in creating an efficient device. Because of manufacturing limitations, there are restrictions for the fin thickness to fin gap. For a .5mm thick fin, the fin spacing must be 3 times that thickness at .15mm. Very thin fins are the most effective where the proper manufactured spacing limits are met. Understanding

these restrictions, fin height and thickness are two important parameters to optimize a heat sink. Furthermore, it was found that a base plate thickness of 5mm-7.5mm creates an optimal result.

The second portion of this paper focused on experimentally characterizing high performance heat sinks in forced-convection, first with one heat sink and secondly with two heat sinks. Measurements showed that at power input of 150 watts and average air velocity of 3 m/s, that maximum temperatures for one or both of the heat sinks stayed below 70°C. Along with respectable thermal contact resistance values, a 150 watt electronic device can safely be cooled under such conditions. Furthermore, it was found that a gap spacing between two heat sinks has minimal affect on the overall thermal resistance of the heat sink. Finally, Nusselt number correlations were determines for each heat sink. The convection coefficient values can now be predicted using these correlations without having to run an experiment. Knowledge of the convection coefficient allows for any air speed and gap spacing to be predicted.

Finally, a study was done using SolidWorks® and ANSYS® to find an optimal geometric layout of 4, equal power producing aluminum chips mounted on a copper heat spreader. This optimized geometric layout can be added on top of any heat sink to create the most efficient cooling system possible. Results from ANSYS showed that:

1) Larger power producing chips are ideal
2) A base spreader thickness of 5mm-7.5mm is ideal
3) The spacing between the aluminum chips is less relevant
4) The larger the wetted surface area of the heat spreader, the more efficient the device.

REFERENCES

[1] Website: http://en.wikipedia.org/wiki/Heat_sink

[2] Frank P. Incropera & David P DeWitt. Fundamentals of Heat and Mass Transfer, 2002 John Wiley & Sons, Inc

[3] Website: http://www.biberthermal.com/Reference_Links/Publications_List/isps99paper.pdf

[4] Dr. Kuznetsov, Heat Transfer Theory Applications, MAE 505, North Carolina State University 2008

[5] Website: http://en.wikipedia.org/wiki/Voltage

[6] Website: http://hardwaresecrets.com/article/274/2

[7] Website: http://en.wikipedia.org/wiki/Thermal_resistance

[8] Cengel & Boles. Thermodynamics, An Engineering Approach, 5th Edition, 2006

[9] Website: http://en.wikipedia.org/wiki/Voltage

[10] Website http://en.wikipedia.org/wiki/Film_Temperature

[11] Professor Richards D. Gould, MAE 310: Heat Transfer Fundamentals, Notes

[12] Lian-Tuh Yeh & Richard C. Chu. Thermal Management of Microelectronic Equipment, pages 185-190, © 2002

APPENDIX

APPENDIX A: GEOMETRIC HEAT SINK OPTIMIZATION (EQUATIONS)

A finite element energy balance shows:

$$\dot{E}_{in} = \dot{E}_{out} \tag{A.1}$$

Where a basic heat transfer conduction equation for a finite element states:

$$q_x = -kA_C\left[\frac{dT}{dx}\right]_X \tag{A.2}$$

$$q_{x+dx} = -kA_C\left[\frac{dT}{dx}\right]_{X+dX} \tag{A.3}$$

$$q_{conv} = hA_s(T - T_\infty) \tag{A.4}$$

By adding all the components into the energy balance:

$$kA_C\left[\frac{dT}{dx}\right]_{X+dX} - kA_C\left[\frac{dT}{dx}\right]_X - hpdx(T - T_\infty) = 0 \tag{A.5}$$

$$\frac{d^2T}{dx^2} - \frac{hp}{kA_c}(T - T_\infty) = 0 \tag{A.6}$$

A parameter θ can be introduced:

$$\theta = T(x) - T_\infty \tag{A.7}$$

Therefore, combining (A.7) and (A.8):

$$\frac{d^2\theta}{dx^2} - \frac{hp}{kA_C}\theta = 0, \text{ where } m^2 = \frac{hp}{kA_C} \tag{A.8}$$

Thus, the temperature distribution can be written as:

$$\frac{d^2\theta}{dx^2} - m^2\theta = 0 \tag{A.9}$$

Boles in: Thermodynamics, An Engineering ApproachThermodynamics, An Engineering Approach states:

$$\theta(x) = C_1 e^{-mx} + C_2 e^{mx} \tag{A.10}$$

A boundary condition at x = 0 reveals the result:

$$\theta(b) = C_1 + C_2 \tag{A.11}$$

Analyzing the boundary conditions, it can be said that:

$$\theta(x) = \theta_b e^{-mx} \tag{A.13}$$

And can be re-written as:

$$T(x) - T_\infty = (T_b - T_\infty)e^{-mx} \tag{A.14}$$

$$e^{-mx} = \frac{T(x) - T_\infty}{T_b - T_\infty} \; and \; m = \sqrt{\frac{hp}{kA_c}} \tag{A.15}$$

By taking the derivative of (A.14), and plugging it into (A.2), the result yields:

$$q_x = -kA_c(T_b - T_\infty)e^{-mx}(-m) \tag{A.16}$$

And plugging in “m” into (A.16):

$$q_x = \sqrt{hpkA_c}(T_b - T_\infty)e^{-mx} \tag{A.17}$$

The conduction into the fin at x = 0, is the equation for fin heat dissipation.

$$q_{fin} = \sqrt{hpkA_c}(T_b - T_\infty) = \sqrt{hpkA_c}\theta_b \tag{A.18}$$

If the fin is not present, the total heat generated can easily be denoted as a one dimensional convection problem:

$$q_{without\ fin} = hA_c(T_b - T_\infty) = hA_c\theta_b \tag{A.19}$$

Plugging in (A.18) & (A.19), fin effectiveness can be written as:

$$\varepsilon = \frac{q_f}{q_{w/out}} \tag{A.20}$$

Yielding the final result for fin performance by:

$$\varepsilon = \sqrt{\frac{pk}{hA_C}} \tag{A.21}$$

Finally, fin efficiency can be found by the simple equation:

$$\eta_{fin} = \frac{q_f}{q_{\max}} \tag{A.22}$$

APPENDIX B: EXPERIMENTAL HEAT SINK OPTIMIZATION (EQUATIONS)

Voltage for the system can be found by:

$$V = \sqrt{P R} \tag{B.1}$$

And thermal resistance can be found by:

$$R_{thermal} = \frac{\Delta T_{\max}}{P} \tag{B.2}$$

Correlated temperature dependant parameters were generated in EXCEL:

Dynamic viscocity, (B.3)

$$\mu = 2x10^{-14}(T^3) - 6x10^{-11}(T^2) + 8x10^{-08}(T) - 2x10^{-7}$$

Kinematic Viscocity, (B.4)

$$\nu = 8x10^{-11}(T^2) + 5x10^{-8}(T) - 5x10^{-6}$$

Thermal Conductivity, (B.5)

$$k = 7x10^{-5}(T) + .0046$$

Prandtl Number, (B.6)

$$Pr = -3x10^{-7}(T^2) + 8x10^{-5}(T) + .7166$$

Where the hydraulic diameter needed to calculate a Reynolds Number in a Square duct:

$$d_h = \frac{4A_c}{P} \tag{B.7}$$

The experimental coefficient of convection can be found by:

$$h_{exp} = \frac{q_{conv,fin}}{A_{wetted}(T_{base} - T_\infty)} \tag{B.8}$$

The general Nusselt Number correlation is:

$$Nu = C_1 Re^m Pr^n \tag{B.9}$$

Where Reynolds Number can be found by:

$$Re = \frac{\overleftarrow{V_{fin}} L_C}{\nu} \tag{B.10}$$

It was found that the expected fin velocity can be calculated by:

$$\overleftarrow{V}_{fin,expected} = \frac{\overleftarrow{V}_{in,avg} A_{c,duct}}{A_c} \tag{B.11}$$

By weighting each of the velocity readings upstream by their relative position, the expected fin velocity can be calculated by:

$$\overleftarrow{V}_{fin,expected} = \frac{\sum_{i=1}^{40} \sum_{i=1}^{40} V_{i,j} A_{i,j}}{A_c} \tag{B.12}$$

Each of the temperature dependant correlations use an experimental film temperature:

$$T_{film}(K) = \frac{T_{max} + T_{ambient}}{2} \tag{B.13}$$

Nusselt Number can also be found using the convection coefficient related equation:

$$Nu = \frac{hL_c}{k_{air}} \tag{B.14}$$

To solve the Nusselt Number Correlation, a least-squares regression is used:

$$\underbrace{\log(Nu)}_{\hat{Z}} = \underbrace{mlog(Re)}_{\hat{x}} + \underbrace{mlog(\mathrm{Pr})}_{\hat{y}} + \underbrace{log(\mathrm{C1})}_{\hat{C}} \tag{B.15}$$

Where the values can be predicted by:

$$E = e^2 = \sum_{i=1}^{N} \left(z_i - Ax_i - By_i - C\right)^2 \tag{B.16}$$

Expanding (B.16) yields:

$$A\sum_{i=1}^{N} x_i^2 + B\sum_{i=1}^{N} x_i y_i + C\sum_{i=1}^{N} x_i = \sum_{i=1}^{N} x_i z_i \tag{B.17}$$

$$A\sum_{i=1}^{N} x_i y_i + B\sum_{i=1}^{N} y_i^2 + C\sum_{i=1}^{N} y_i = \sum_{i=1}^{N} y_i z_i \tag{B.18}$$

$$A\sum_{i=1}^{N} x_i + B\sum_{i=1}^{N} y_i + C\sum_{i=1}^{N} 1 = \sum_{i=1}^{N} z_i \tag{B.19}$$

And the resulting matrix carries the form, which allows to simultaneously solve all test cases:

$$\begin{bmatrix} \sum x_i^2 & x_i y_i & \sum x_i \\ \sum x_i y_i & \sum y_i^2 & \sum y_i \\ \sum x_i & \sum y_i & N \end{bmatrix} * \begin{bmatrix} A \\ 1/3 \\ C \end{bmatrix} = \begin{bmatrix} \sum x_i z_i \\ \sum y_i z_i \\ \sum z_i \end{bmatrix} \tag{B.20}$$

By looking at the form of (B.15), into the matrix shape of (B.20), this yields:

$$\begin{bmatrix} \sum_{i=1}^{N}(\log\ Re)^2 & \sum_{i=1}^{N}(logRe) \\ \sum_{i=1}^{N}(logRe) & N \end{bmatrix} * \begin{bmatrix} A \\ C \end{bmatrix} = \begin{bmatrix} \sum_{i=1}^{N}(logRe * logNu) \\ \sum_{i=1}^{N}(logNu) \end{bmatrix} \quad \text{(B.21)}$$

The flat plat Nusselt Number correlation:

$$Nu = 2.587Re^{.3043}Pr^{1/3} \quad \text{(B.22)}$$

Considering Reynolds Number in a square duct:

$$Re = \frac{\overleftarrow{Vd_h}}{\nu} \quad \text{(B.23)}$$

Nusselt is rewritten as:

$$Nu = \frac{hd_h}{k_{air}} \quad \text{(B.24)}$$

The resulting square duct Nusselt Correlation is:

$$Nu = .8188Re^{.3016}Pr^{1/3} \quad \text{(B.25)}$$

To obtain a Nusselt Correlation for the second heat sink for a forced-convection test:

$$Nu = C_1 Re^m \left(\frac{H}{t}\right)^m \left(\frac{L}{t}\right)^n Pr^{1/3} \quad \text{(B.26)}$$

Where Nusselt and Reynolds can be found in a new form by:

$$Nu = \frac{ht}{k} \quad \text{(B.27)}$$

$$Re = \frac{\dot{m}w}{\mu} \quad \text{(B.28)}$$

The resulting 2nd heat sink Nusselt correlation came out to be:

$$Nu = .00569Re^{.4061}\left(\frac{H}{t}\right)^{-4.3356}\left(\frac{L}{t}\right)^{-.729}Pr^{1/3} \tag{B.29}$$

APPENDIX C: COPPER HEAT SPREADER ANALYSIS (EQUATIONS)

The gap spacing can b e calculated relative to the size of the aluminum power chip by:

$$s = \frac{w - 2d}{3} \tag{C.1}$$

Where the heat flux value that is used in ANSYS® can be found by:

$$q'' = \frac{q}{A_{s,Al}} \tag{C.2}$$

From (C.1) & (C.2), the overall thermal resistance can be calculated using:

$$R = \frac{\Delta T}{q'' A_{s,Al}} \tag{C.3}$$

The thermal resistance due to convection can be found by:

$$R_{conv} = \frac{1}{hA_{s,Cu}} \tag{C.4}$$